Polymeric and Nanoparticle-based Photonic Crystals for Distributed Feedback Lasers

by

Francesco Scotognella

A dissertation submitted for the degree of

DOTTORE DI RICERCA

in

SCIENZA DEI MATERIALI

at the

DIPARTIMENTO DI SCIENZA DEI MATERIALI
UNIVERSITÀ DI MILANO BICOCCA

Supervisor
Prof. Riccardo Tubino

DECEMBER 2009

Abstract

The development of new smart structures to provide optical feedback mechanisms paves the way to the realization of novel laser emitters. An approach that has been attracting the interest of many researchers is the distributed feedback (DFB), provided by a periodic dielectric modulation along the propagation direction of the light. Such structures, namely photonic crystals, are the optical analogues of electronic semiconductors. In these systems a periodicity (comparable with the optical wavelengths) in the dielectric constant along one, two or three spatial dimensions generates stopgaps, photonic band gaps and slow photons. On the other side, point, line, bend and planar defects give rise to intra-gap states.

To obtain laser emission, both an active material that exhibits strong stimulated emission and an optical feedback are necessary. For the first requirement, a variety of state-of-the-art conjugated molecules and polymers are available combining easy manufacturing with high gain properties. For the second one, the optical feedback, several photonic structures are reported in literature. Focusing on DFB provided by one dimensional photonic structures, two model systems are reported, namely corrugated substrates (1D gratings) and multilayer structures respectively. 1D DFB gratings are extensively studied: several works report structures with very high performance in term of lasing threshold and line narrowing. Nevertheless, expensive and complicated lithographic or UV embossing procedures are required to make such gratings. Although performances of common multilayer systems are still not comparable with the gratings, multilayer devices are really promising for low-cost technological applications, since their manufacturing employs standard and basic techniques.

With this perspective, we have fabricated different types of multilayers. Polymeric 1D PCs have been grown on rigid and flexible substrates and have been doped with the laser dye Rhodamine 6G. Moreover, we have fabricated nanoparticle-based 1D PCs, which we have infiltrated with Rhodamine 6G or with the polymer emitter poly (phenylene vinylene). These systems behave as a DFB laser and stimulated emission has been observed. We have studied the laser characteristics and the observed thresholds are lower than the ones reported in literature for other types of organic lasers.

In conclusion, we have employed various materials to manufacture multilayer DFB lasers. These materials give different interesting properties, as for example flexibility and porosity. Porous PCs shift the position of the photonic band gap as a function of the concentrations of several vapours and liquids: this gives the possibility to make "tunable" DFB laser by increasing/decreasing the concentration of a specific vapour or liquid, for laser switches and sensors. The morphological and optical characterization provided a comprehensive analysis of the fabricated lasers and give detailed guidelines for the improvement of such systems for application in real devices.

Contents

Chapter 1
Introduction

Among the most common words derived from the technology (and the Materials Science) is the term laser. The word “laser” is shorthand for the phrase “light amplification by the stimulated emission of radiation”. Laser-based devices, for example, are CD and DVD players, laser writers (and laser printers), bar code readers and industrial laser cutters. Nowadays, lasers are heavily used in optical communications and in medicine, for kidney stone treatment, eye treatment, dentistry, bloodless and precision surgery [1,2].

From the historical point of view, in 1917 Albert Einstein first proposed the process that makes lasers possible called Stimulated Emission. In 1947, Gabor developed the theory of holography that requires laser light for its realization; he received in 1971 the Nobel Prize in Physics for this work. The first papers about the maser were published in 1954 as a result of investigations carried out simultaneously and independently by Charles Hard Townes and his co-workers at Columbia University in New York and by Basov and Prokhorov at the Lebedev Institute in Moscow. Their work continued throughout the '60s and the '70s. They were awarded the 1964 Nobel Prize in Physics. The optical maser or the laser dates from 1958, when the possibilities of applying the maser principle in the optical region were analyzed by Schawlow and Townes as well as in the Lebedev Institute. Laser spectroscopy was developed by Schawlow and his co-workers at Stanford University and, around the same time, Bloembergen and his co-workers developed nonlinear optics which is a very special application of laser spectroscopy. Schawlow, Bloembergen, with the Swedish scientist Kai M. Siegbahn, won the Nobel Prize in Physics in 1981. The first laser was operating in 1960. It was a ruby laser generating strong pulses of red light. Alferov and

Kroemer proposed in 1963, independently of each other, the principle for semiconductor heterostructures to be used later in semiconductor laser which today, by far, is the most common laser (Noble Prize in Physics, 2000). Other Nobel Prizes in Physics related to the laser are in 1997 (Chu, Cohen-Tannoudji and Phillips**,** for their developments of methods to cool and trap atoms with laser light) and 2005 (Glauber, Hall and Hänsch, for their contributions to the development of laser-based precision spectroscopy, including the optical frequency comb technique). Moreover, it is noteworthy the 1999 Nobel Prize in Chemistry to Ahmed H. Zewail for his studies of the transition states of chemical reactions using femtosecond spectroscopy [3].

The most common lasers today are tiny chips of semiconductor compounds such as Gallium Arsenide, but materials developments have played a crucial role in the development of new lasers. Organic semiconductors combine novel optoelectronic properties, with simple fabrication and the scope for tuning the chemical structure to give desired features, making them attractive candidates as laser materials, as well as for the other applications described in this issue. The rapid recent development of organic semiconductor lasers builds on the development of organic light-emitting diodes, which are now commercially available in simple displays. It opens up the prospect of compact, low-cost (even disposable) visible lasers suitable for applications from point of care diagnostics to sensing.

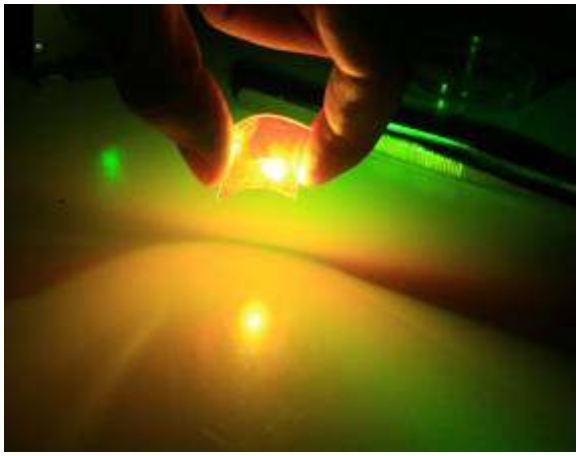

Fig. 1.1. Organic dye laser fabricated on a flexible substrate.

Lasing from optically pumped small molecules as well as optically pumped organic molecular crystals was developed over 30 years ago [4-6]. Only in 1992 that lasing was demonstrated from solutions containing conjugated polymers and not until 1996 that laser-like emission in a solid conjugated polymer was demonstrated [7,8].

In general, a laser must possess at the very least two components. The first is an active emissive material, which should exhibit a good stimulated emission cross-section, and secondly a structure which supplies a feedback mechanism. For the feedback mechanism, diffractive resonators such as photonic crystals [9,10], opportunely doped with active materials, are commonly employed to fabricate distributed feedback (DFB) lasers [11-14]. Such are commonly planar structures in which optical feedback is provided by a nano-patterned surface, either as a substrate or directly embossed in the active layer [15]. Recently, interest in vertical one-dimensional photonic crystals (1D PCs) or Distributed Bragg Reflectors (DBRs) has surfaced within the materials chemistry community in an attempt to exploit the intense broadband reflectivity such materials offer for a variety of applications, both conventional and

unconventional. Recent reports have focused on the fabrication of "functional" DBRs by employing building blocks ranging from nanoparticles to clays to polyelectrolytes and zeolites [16-18]. In such systems, the photonic structures exhibit the common DBR characteristics of intense and broadband reflectivity but in addition are also imparted the added functionality of their respective functional building blocks. For example, for DBRs fabricated purely from nanoparticles of SiO_2 and TiO_2, significant mesoporosity as well as the rich and versatile surface chemistry of SiO_2 and TiO_2 become available. The mesoporosity of the nanoparticle DBR structure was pivotal to the study as it allowed for the uptake of a sufficient quantity of laser dye and also ensured that the dye was spatially well dispersed in order to prevent fluorescence self-quenching [19].

The aim of this thesis is the fabrication, the morphological and the optical characterization of different of DFB lasers, where the "building-block" that we have changed has been the one dimensional photonic crystal employed to provide the optical feedback. Dye-doped polymeric 1D PCs have been grown on glass and cellulose substrates to make all-plastic rigid and flexible DFB lasers. Nanoparticle-based 1D PCs have been infiltrated with an organic dye and a polymer precursor, followed by *in situ* polymerization, to make porous DFB lasers. The optical properties, with a particular focus on the laser threshold and laser characteristics, are discussed.

Moreover, by varying the "building blocks", we have changed the functionality of the DFB lasers, i.e. the flexibility and the porosity. The porosity bodes well for future work whereby adsorption-desorption of vapours and liquids can be gainfully employed as a means to dynamically tune the frequency of the laser emission, suggesting exciting opportunities for new kinds of displays and sensors.

Chapter 2
Organic Semiconductor Lasers

2.1 Active Materials

2.1.1. Types of Organic Semiconductors

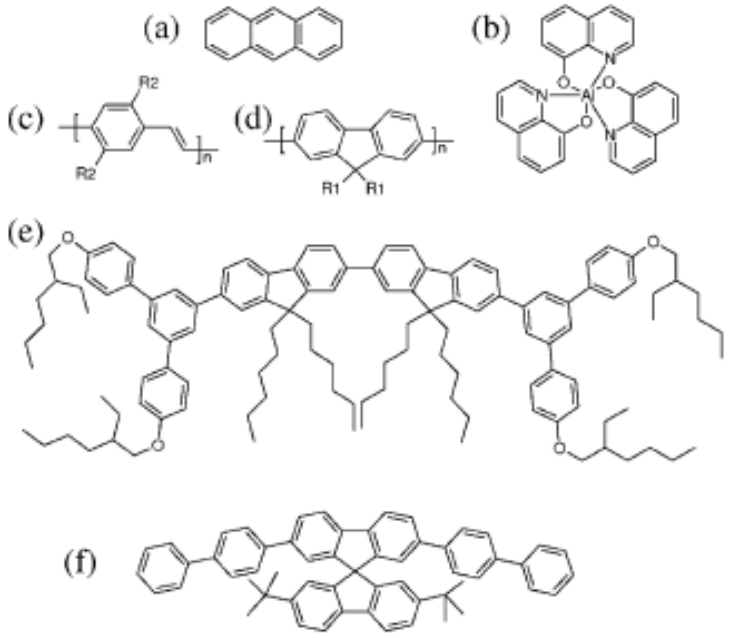

Figure 2.1: Chemical structures of typical organic semiconductors used for lasers: (a) anthracene; (b) aluminum tris(quinolate); (c) generic poly(para-phenylene vinylene) derivative; (d) generic polyfluorene derivative; (e) bisfluorene cored dendrimer; (f) spirolinked oligomer.

There are several types of organic semiconductors relevant to lasing, and their classification is by a combination of structural features and how they are

processed. Organic semiconductors are conjugated molecules, with the semiconducting properties arising from the overlap of molecular orbitals. Early work focused on single crystals of materials such as anthracene, Figure 2.1a [6]. When sufficiently high voltages were applied, light was emitted, but the difficulties of growing and handling these materials meant that it was the discovery by Tang and Van Slyke [20] of efficient electroluminescence in evaporated films of small molecule organic semiconductors that attracted serious interest in using the materials for light emission. We will refer to this class of organic semiconductor as small molecules, and an example is aluminum tris(quinolate) (Figure 2.1b).

There are three other types of organic semiconductors that have been studied as laser materials. The first is conjugated polymers. These long chain-like molecules have alternating single and double bonds giving electron delocalization along the molecule. Two families of conjugated polymer have been studied particularly extensively: the poly(phenylene vinylene)s (Figure 2.1c) and the polyfluorenes (Figure 2.1d) [8,21-24]. A major difference from small molecules is that conjugated polymers can be deposited from solution by processes such as spin-coating and ink-jet printing, giving even simpler fabrication of devices. Two further types of organic semiconductor have been studied for lasers (and LEDs). The first of these is conjugated dendrimers [25]. These typically consist of a chromophore at the core, conjugated branches (dendrons), and surface groups. The core defines the key electronic properties such as the color of light emission, while the surface groups confer solubility. The highly branched structure contrasts with the much more linear structure of conjugated polymers. An example of a conjugated dendrimer is shown in Figure 2.1e. The material shown is a first generation dendrimer, so it has just one level of branching. It consists of a bisfluorene core with meta-linked biphenyl dendrons and ethylhexyloxy surface groups. Dendrimers with non

conjugated dendrons and laser dyes incorporated into a dendritic host have also been studied for lasing and amplification [26,27]. Another type of organic semiconductor is the spiro-compounds. These consist of two oligomers coupled to each other by a spiro linkage, and an example is shown in Figure 2.1f [28-31].

2.1.2. Organic Semiconductor Photophysics

There are many aspects of the photophysics of organic semiconductors that are relevant to lasers. First, the materials absorb light very strongly, so at the peak of the absorption spectrum, a thin film only 100 nm thick can absorb 90% of the light incident on it. This means that light can be absorbed in very short distances and, since stimulated emission is closely related to absorption, also means that very strong gain is possible. Both attributes have been demonstrated very clearly in Tessler's work showing lasing using a conjugated polymer film only 100 nm thick [8]. The strong absorption and gain have a major impact on resonator design. The fluorescence spectra of organic semiconductors are broad and, in addition, can be tuned by changing the chemical structure to give light emission across the visible spectrum and into the near ultraviolet and infrared. The broad spectra mean that organic semiconductor lasers can be tuned over a significant spectral range and also mean that these materials are capable of short pulse generation and broadband optical amplification. For both LEDs and lasers, it is desirable to use materials that emit light efficiently. The efficiency of light emission can be described quantitatively by the photoluminescence quantum yield (Φ_{PL}), which is defined as the ratio of the number of photons emitted by a sample to the number of photons absorbed. For thin films of organic materials, it can be conveniently measured by placing a thin film in an integrating sphere, which collects the light emitted in all directions.

Considerable effort has gone into increasing the photoluminescence efficiency of thin films of organic materials. In particular, a range of strategies have had to be developed to control intermolecular interactions. At high concentrations or in the solid state, conjugated organic molecules can interact with their neighbors, leading to the formation of (physical) dimers, aggregates, or excimers, which can quench light emission. Hence many laser dyes, which are extremely fluorescent materials in dilute solution, are almost non-emissive in the solid state [11].

2.2. Gain in Organic Semiconductors

A laser consists of a medium capable of amplifying light (known as the gain medium) in a resonator. In this subsection, we will consider the origin and properties of the gain in organic semiconductors, while the effect of the resonator will be discussed in the next section. When a photon is incident on a material, it can cause an electron to be excited from a lower to a higher energy level, the process we know as absorption. Similarly, when a photon is incident on a material that has already been excited, it can cause an electron to fall from a higher to a lower energy level and the emission of another photon. This process is known as stimulated emission, and its existence was first proposed by Einstein based on thermodynamic considerations. Further information about this discovery and laser physics can be found in countless lasers textbooks including those of Siegman and Svelto [32,33]. A crucial point is that the photon emitted has the same phase, frequency, and direction as the incident photon. The fact that an additional photon is released means that there has been amplification of the incident photon. So as light travels through a gain medium, it stimulates the emission of more and more photons and (for small signals) its intensity, $I(z)$, increases exponentially with distance:

$$I(z) = I(z = 0)e^{gz} \qquad (2.1)$$

where g is the wavelength-dependent gain coefficient of the medium. Einstein showed that for a particular transition, the cross sections for absorption and stimulated emission are the same. This means that in order to get more stimulated emission than absorption at a given wavelength, we need to have more molecules excited to the upper state than are in the lower state, a situation known as a population inversion. The gain coefficient is simply the product of the stimulated emission cross section, σ, and the population inversion density, N, that is, $g = \sigma N$. Inversion cannot be practically achieved in a system with just two energy levels. However, it can be achieved in a system with three or four energy levels.

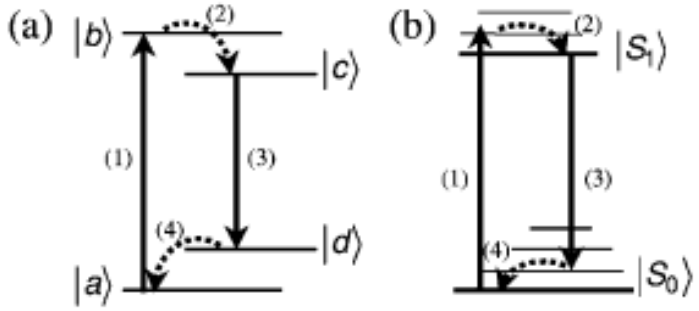

Figure 2.2: Energy level diagrams for optical gain media: (a) energy levels and transitions of a generic four-level laser materials transitions 1 and 3 are optical absorption and emission, and transitions 2 and 4 are thermal relaxations; (b) energy levels of the lowest two singlet states in an organic semiconductor, including the corresponding optical and thermal transitions to those in panel a.

A four-level system is shown in Figure 4a. Light excites a molecule from the ground state to an excited state (transition 1 in the figure), and it then rapidly relaxes to another energy level (transition 2). The lasing transition (3) then occurs down to a fourth level, which is above the ground state. There is then a rapid return to the ground state via transition 4. The advantage of a four-level system is that there can be a population inversion between levels $|c\rangle$ and $|d\rangle$, even when most molecules are in the ground state, so lasing can be obtained for a very low rate of excitation, with a consequent low threshold for lasing.

The energy levels in a typical organic semiconductor are shown in Figure 4b. The figure shows the ground state and first excited singlet state. Each of these electronic energy levels is subdivided into vibronic sublevels. The spacing of these sublevels is approximately 0.2 eV, so at room temperature, there is little thermal excitation from the lowest level. Light can excite the molecule from its ground state to an excited vibrational level of the singlet manifold (corresponding to transition 1 in Figure 4a). This will be followed by rapid vibrational cooling to the bottom of the singlet manifold (transition 2). Lasing can then take place by transition 3 to a vibrationally excited level of the ground state manifold, followed by vibrational relaxation (transition 4). Hence the energy levels of organic semiconductors enable them to behave as four-level lasers, with associated low thresholds. It also explains why the emission occurs at longer wavelength than the absorption.

There is an additional factor that contributes to separating the absorption and emission, especially in the solid state. In a film of an organic semiconductor, there will be a distribution of environments and hence a distribution of energy levels. This is particularly the case in conjugated polymers, which can have a great deal of conformational disorder, giving segments with a range of energy levels. We can regard the sample as consisting of many different sites of different energy. We initially excite molecules or segments of molecules with a

wide range of site energies, but energy is rapidly transferred to the lowest energy molecules or segments. This has been elegantly described in terms of a Gaussian disorder model by Bässler's group, and the associated red shift of emission as a function of time has been observed experimentally [34]. Importantly, much of the shift occurs in the first few picoseconds after excitation (though, of course, the dispersive nature of the process means that it continues over many orders of magnitude of time). This energy-transfer process means that emission occurs from the lowest energy sites in the sample and so increases the separation between absorption and fluorescence. This in turn is helpful for lasing because it reduces the amount of absorption at the lasing wavelength. The separation between absorption and emission can be increased further by blending two different materials with different energy gaps. Light absorbed by the wider energy gap material will lead to energy transfer to the lower energy gap material and emission from that material. One example is the use of a blend of the red laser dye 4-(dicyanomethylene)-2-methyl-6-(4-dimethylaminostyryl)-4H-pyran (DCM) as a dopant in the green host material tris(8-hydroxyquinoline) aluminum (AlQ_3) [35]. Another example is green-emitting polymers in a blue host [36]. The energy transfer process has been studied and been shown to be by the Förster mechanism. A closely related way of separating the emission from the absorption is to use a copolymer consisting of wider and narrower energy gap segments, and this has been demonstrated successfully for lasers and optical amplifiers [37,38].

The presence of gain in a material is an essential condition for it to be possible for lasing to occur. There have been two main approaches to studying gain in potential organic semiconductor laser materials. The first is by transient absorption measurements. The second is by measurements of amplified spontaneous emission (ASE). Transient absorption measurements are an all-optical approach to ultrafast measurements of photoexcitations. The sample is

excited by a short pump pulse, which generates photoexcitations, and a time-delayed probe pulse is then used to measure the resulting change in transmission of the sample due to the formation of the photoexcitations. By changing the time delay between the pump and probe pulses, one can measure the transmission as a function of time with a time-resolution comparable to the duration of the laser pulses used (typically 100 fs). The newly formed photoexcitations absorb in some parts of the spectrum, while in other parts of the spectrum there is a reduction of absorption (bleaching) due to the reduced population in the ground state. If there is gain in the sample, the probe will be amplified by stimulated emission and be stronger after passing through the sample. Hence transient absorption provides a powerful means for studying photoexcitations and their time evolution, together with gain and its time evolution. An example of such a measurement is shown in Figure 2.3. The decrease in absorption from 1.8 to 2.15 eV is mainly due to stimulated emission. The graph therefore shows the spectral and temporal evolution of gain, including the red shift with time mentioned in the previous paragraph. There are three main factors that determine the overall gain spectrum. They are the gain spectrum of the material, the ground-state absorption, and excited-state absorption. The overall gain is the material gain minus absorption.

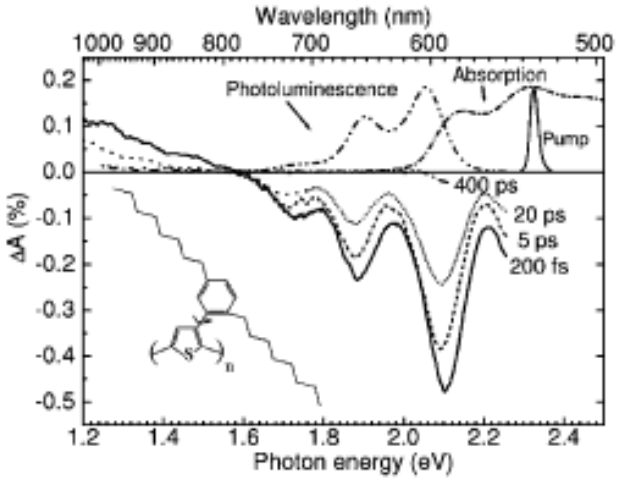

Figure 2.3: Transient absorption spectra of poly [3-(2,5-dioctylphenyl)-thiophene]; chemical structure inset (from *Journal of Luminescence*, vol. 76 and 77, A. Ruseckas, M. Theander, L. Valkunas, M. R. Andersson, O. Ingänas, and V. Sundström, "Energy transfer in a conjugated polymer with reduced interchain coupling", pp 474-477, Copyright 1998).

Early work toward making conjugated polymer lasers involved making transient absorption measurements on members of the poly (p-phenylene vinylene) family of polymers. In the first of these studies, no gain was observed, probably due to the material used or the excitation wavelength (310 nm). In the other study, the gain was extremely short-lived, and this was attributed to the rapid formation of intermolecular photoexcitations with strong photoinduced absorption overlapping the gain. In subsequent work, with improved materials, there have been numerous reports of gain in organic semiconductors and its dynamics. These studies have confirmed that very high gain is possible. They have also shown that gain lifetimes are usually short, on the picosecond time scale. This presents a challenge for lasers, because a short excited-state lifetime means that a high pump rate is needed to maintain a

population inversion. However, too high a pump rate leads to exciton-exciton annihilation, which is an undesirable nonradiative decay process.

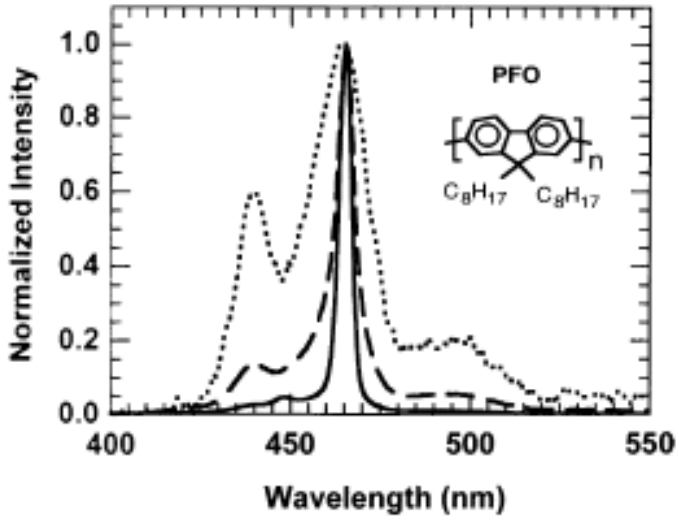

Figure 2.4: The change in spectral shape with increasing excitation density of the edge emission from a PFO film. The normalized spectra show a significant spectral gain narrowing at high excitation densities (G. Heliotis, D. D. C. Bradley, G. A. Turnbull, and I. D. W. Samuel, "Light amplification and gain in polyfluorene waveguides", pp 415-417, Copyright 2002 American Institute of Physics).

The other main method for measuring gain is by ASE. This involves making a slab waveguide of an organic semiconductor, exciting it with pulsed pump-laser light in a stripe near the edge of the sample, and looking at the light emitted from the edge of the sample. Some of the light emitted by the material is waveguided along the length of the excitation stripe. This guided spontaneous emission can be amplified by stimulated emission before being emitted from the edge of the film. Light at the peak of the gain spectrum of the material will be amplified more than other light, leading to a spectrally narrowed emission (typically a few nanometers full width at half-maximum) above a particular

pumping intensity. The change in spectral shape with excitation density is illustrated in Figure 2.4.

In the case of ASE, spontaneous emission within the film acts as the "probe pulse". One must therefore use an indirect method to measure the gain of the material. The wavelength dependent output intensity, *I(λ)*, of the ASE is given by the relationship

$$I(\lambda) = \frac{A(\lambda) I_p}{g(\lambda)} e^{(g(\lambda) l) - 1} \qquad (2.2)$$

where *A(λ)* is a constant related to the emission cross section, I_p is pumping intensity, and *l* is the length of the stripe. So, by monitoring the intensity of the line-narrowed emission as a function of the stripe length, one may calculate the net gain, *g(λ)*. This method was initially applied to the inorganic semiconductor cadmium sulfide [39] but has since been widely applied to determine the gain of organic semiconductors [40]. Additionally, by progressively moving the stripe away from the edge of the film, it is possible to measure the waveguide losses of light propagating through an unpumped region of the film. Waveguide losses in conjugated polymers typically lie in the range of 3-50 cm^{-1}, with the lower end of the range being for copolymers. Even lower losses (<1 cm^{-1}) have been reported in blended organic thin films [41]. Net gains have been measured for a wide range of materials and can be over 60 cm^{-1} at modest pumping densities of 4 kW cm^{-2} [42]. Measurements of ASE are generally very useful because they are relatively simple to perform and the geometry is close to that used in waveguide lasers. However, transient absorption gives more insight into the factors controlling the gain, can readily probe the entire emission spectrum, and gives the gain dynamics. The high gain of organic semiconductors has several consequences: very compact lasers can be made, the lasers are tolerant

of minor fabrication defects, and the materials can also be used to make compact optical amplifiers [11].

2.3. Laser Resonators

2.3.1. Generic Properties of Laser Resonators

As mentioned in the introduction, every kind of laser consists of two basic elements. First there is an optical gain medium that amplifies the light via stimulated emission and second an optical feedback structure that repeatedly passes a resonant light field through the gain medium to establish a very intense, coherent optical field inside the laser. This optical feedback system is conventionally called the optical resonator or optical cavity. In the very simplest case, this optical cavity may comprise only two mirrors, configured as a Fabry-Perot interferometer, between which the amplifying gain medium is situated (Figure 2.5a). This Fabry-Perot type resonator is the simplest example of a linear cavity that supports a standing-wave optical field between the two mirrors. A second simple configuration for an optical cavity is an optical ring resonator, in which the light circulates as a travelling wave around a closed path defined by three or more mirrors (Figure 5b).

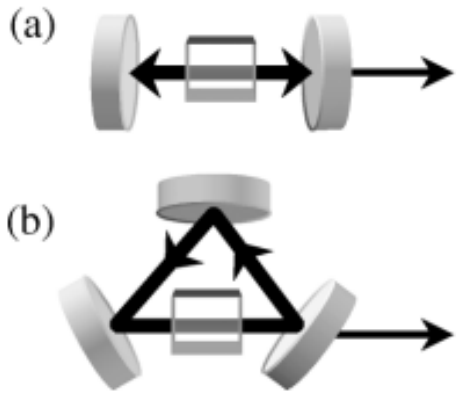

Figure 2.5: Schematic diagrams of generic laser resonator structures: (a) linear Fabry-Perot cavity, with gain medium located between two parallel mirrors, supporting a standing-wave resonant light field; (b) three mirror ring cavity, supporting a travelling-wave resonant light field through the gain medium.

There are many variations of these two basic cavity structures, but they ultimately all impose two basic properties upon the oscillating laser light field. First, they define the allowed resonant frequencies of the device (within the constraint of the gain medium's emission spectrum) and hence the wavelengths of the laser field. Second, they define the spatial characteristics of the laser beam that is output from the resonator. These defining characteristics of the laser light arise from the fundamental boundary condition of the laser field: the laser light field must be unchanged in both amplitude and phase following one round-trip of the optical cavity. This requirement leads to a discrete set of resonant frequencies for a given laser resonator, each of which must have an integer number of optical cycles, or wavelengths, in one round-trip of the cavity. These frequencies are known as the longitudinal, or axial, modes of the resonator. The optical cavity will also define certain transverse mode patterns that are self-replicating following a round trip of the structure. These transverse modes within the laser cavity ultimately determine the transverse light pattern of the emitted laser beam.

The cavity is also key to the power characteristics of the laser and has an impact on both the oscillation threshold and the output efficiency. To achieve a sustained oscillation in a laser, amplification in the gain medium must (at least) balance out with the optical loss (dissipation) during each round-trip of the cavity. The intensity of light passing through a gain medium of length l is amplified by a factor $e^{\sigma Nl}$. The magnitude of the population inversion density, and hence the gain, depends on the external pumping rate. In the case of steady-state optical pumping, $N = P_p\tau /(h\nu V)$, where, P_p is the pump power, τ is the excited-state lifetime, $h\nu$ is the pump photon energy, and V is the volume of the population inversion. For pulsed optical pumping, with a pump pulse of energy E_p and a duration much less than the excited-state lifetime, the initial excitation density is $N(t=0) = E_p\tau /(h\nu V)$ and decays away with time due to spontaneous and stimulated emission and various nonradiative decay paths. The optical loss in the resonator, meanwhile, is due to a product of transmission losses through each of the mirrors and any other absorption and scattering losses in the cavity components. The round-trip fractional optical loss β may therefore be written as

$$\beta = 1 - e^{-\gamma} \prod R_i \qquad (2.3)$$

where R_i is the reflectivity of the i^{th} mirror in the cavity and γ is a loss coefficient embodying all scattering and absorption losses.

Thus as light propagates round a ring laser resonator, its intensity will change by a factor $e^{\sigma Nl}e^{-\gamma}\prod R_i$ in each round trip. (For a linear laser resonator the intensity will change by a factor $e^{\sigma Nl}e^{-\gamma}\prod R_i$, due to the double pass through the gain medium in each round trip.)

If the pumping rate is too low, then the gain from stimulated emission cannot exceed the round-trip loss, and a light field cannot build up in the laser cavity. In this case, the excitations in the gain medium are radiated in all directions as

spontaneous emission. At a certain critical pumping rate, known as the threshold rate, the gain balances out the round-trip losses, and

$$e^{\sigma N_{Th} l} e^{-\gamma} \prod R_i = 1 \qquad (2.4)$$

where N_{Th} is the excitation density at threshold. When the pump rate increases beyond this value, a coherent light field will grow inside the laser cavity. Some of this light will leak out as an intense coherent laser beam whose power will rise linearly with the excess pump rate. The lower the loss of the optical cavity, therefore, the lower will be the optical gain required to make the laser oscillate. Low-loss resonators are therefore very attractive for achieving lasing for modest external pumping rates.

The striking change in operation around the lasing threshold can be understood by considering the many "photon modes" into which light may be emitted. Below threshold there may be $\approx 10^6$ to 10^{10} spectral and spatial modes into which the light may be emitted. That is it may be emitted into a wide range of different spatial directions and different wavelengths. As the pump excitation increases, the probability of finding a photon in any one of these modes at a given time rises. The lasing threshold occurs when one of these modes (the one with the lowest cavity losses) exceeds an average of one photon in it at all times. When pumping above this threshold, the stimulated emission into this one mode rapidly builds up to dominate spontaneous emission into all of the others, and the excess pumping energy is efficiently converted into a coherent laser field.

Independent of this requirement for lasing threshold, the resonator also affects the output efficiency of a laser. When pumped above threshold, the output power, P_{out}, from a laser varies with pump power, P_p, as

$$P_{out} = \frac{T_{out}}{\beta} \frac{\lambda_p}{\lambda} \eta_{PL} (P_p - P_{pTh})$$

In Eq 3.5, λ and λ_p are the wavelengths of the laser and optical pump source, η_{PL} is the emission efficiency of the optical gain medium (when under strong excitation), T_{out} is the transmission of a partially reflecting output-coupling mirror, and P_{pTh} is the pump power at threshold. Output efficiencies from a laser are usually expressed as a power slope efficiency, which is the differential efficiency of output power to pumping power, η_{PL} λ_p. Clearly several factors affect the slope efficiency, including the emission efficiency of the gain medium. But one easily engineered parameter is the ratio of useful output-coupling losses to the total roundtrip losses of the cavity. In order to have a highly power efficient laser, one requires that the useful output-coupling losses form a very large fraction of the total losses of the resonator. These total losses may include absorption, scattering, and unwanted transmissions of the resonant light field. In order to optimize the power characteristics of the laser, one would therefore choose to have as low a loss or high quality optical cavity, of which as great a fraction of the loss as possible is due to an element that extracts a useful output beam from the intra-cavity light field.

Laser resonators are, of course, often much more complicated than the very simple generic linear and ring cavities shown in Figure 2.5 and may contain many other elements. Notably there may be other structures that provide additional wavelength selection, control of the polarization state or transverse mode, or even switching elements that may modulate the losses of the resonator. For lasers based on very broad-band gain media, such as organic molecules, it is common to include a highly dispersive element such as a diffraction grating, which will introduce additional substantial losses for all but a narrow band of wavelengths. By changing the properties or orientation of this

dispersive element, one may tune the narrow wavelength band that experiences low loss and hence tune the laser emission throughout the wide gain bandwidth of the gain medium [11].

2.3.2. Type of Laser Resonators

Optically pumped organic semiconductor lasers have been demonstrated in a very wide variety of different resonant structures. These include the "conventional" laser cavities described above, although most work has concentrated on microscopic resonators based on thin films of the organic semiconductor. Organic lasers configured as planar, cylindrical, and spherical microcavities, optical waveguide based cavities, and a remarkable range of diffractive structures have been studied, some of which are illustrated in Figure 2.6. While some of these appear quite different from the generic cavities shown in Figure 2.5, their basic function, in providing resonant feedback through the gain medium, is fundamentally the same. The different geometries of these lasers, however, lead to a rich variety of spectral, spatial, and power properties.

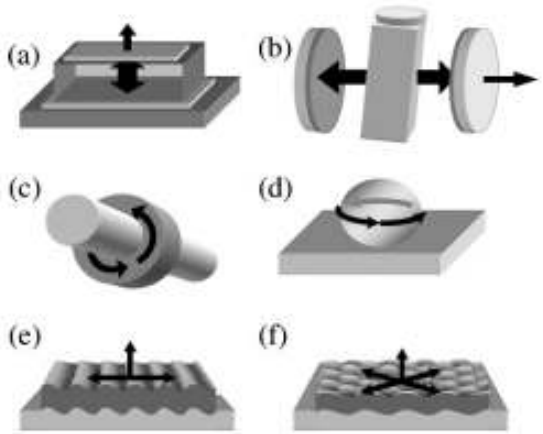

Figure 2.6: Schematic resonators used for organic semiconductor lasers showing propagation directions of the resonant laser field: (a) planar microcavity; (b) Fabry-

Perot dye laser cavity; (c) microring resonator, coated around an optical fiber; (d) spherical microcavity; (e) distributed feedback resonator; (f) 2D DFB/photonic crystal resonator.

Another geometry, very similar to the one described in Figure 2.5e, is based on a one dimensional photonic crystal constituted by layers of two different materials. In the following chapter, we focus on the interesting properties of this type of resonator [11].

Chapter 3
One dimensional Photonic Crystal Lasers

3.1 One dimensional photonic crystals

Photonic crystals are the optical analogues of electronic semiconductors. In these systems a periodicity in the dielectric constant along one, two or three spatial dimensions comparable to optical wavelengths generates stopgaps, photonic band gaps and slow photons. On the other side, point, line, bend and planar defects give rise to intra-gap states [9,10,43-46].

3.2. Origin of the Photonic Band Gap in the 1D case

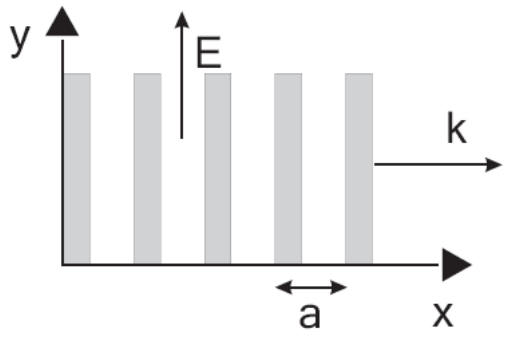

Figure 3.1: 1D photonic crystal with the optical axis along the *x* direction. The gray and white stacks represent the two different materials that form the crystal, while *a* is the lattice constant.

Photonic crystals possess a forbidden gap for photons, analogous to the band gap for electrons in a semiconductor. The origin of this gap is very similar to that of the electronic one. The periodic quantities that make equal electronic and photonic crystals are: the atomic potential in first case and the dielectric

constant in the latter. For simplicity we will examine in detail the 1D case, schematically presented in Fig. 3.1. Considering a non magnetic (μ_r = 1) dielectric system, in which free charges and polarization charges are absent (ρ_{tot} = 0), Maxwell's equations become

$$\begin{aligned} div\,\vec{E} &= 0 \qquad & div\,\vec{B} &= 0 \\ curl\times\vec{E} &= -\frac{\partial\vec{B}}{\partial t} \qquad & curl\times\vec{B} &= \varepsilon\mu\frac{\partial\vec{E}}{\partial t} \end{aligned} \tag{3.1}$$

where $\varepsilon = \varepsilon_0\varepsilon_r$ and $\mu = \mu_0$. Combining the equations and focusing the attention to the 1D case, where light propagates in the x direction in our sample, we obtain

$$\frac{c^2}{\varepsilon_r(x)}\frac{\partial^2\vec{E}}{\partial x^2} = \frac{\partial^2\vec{E}}{\partial t^2} \tag{3.2}.$$

To simplify the treatment we can consider Eq. 3.2 in its scalar form. The dielectric function $\varepsilon_r(x)$ is a periodic function of x, $\varepsilon_r(x) = \varepsilon_r(x+a)$, where a is the lattice constant of the photonic crystal. $\varepsilon_r^{-1}(x)$ is also periodic and can be expanded in a Fourier series as follows:

$$\varepsilon_r^{-1}(x) = \sum_{m=-\infty}^{\infty} k_m e^{i\frac{2\pi m}{a}x} \tag{3.3},$$

where m is an integer and k_m are the Fourier coefficients. Here we suppose that the system does not absorb light, which mean that $\varepsilon_r(x)$ is real and hence that $k_{-m}=k_m^*$. Since $\varepsilon_r(x)$ is periodic, we can use Bloch's theorem, which gives us the eigenmodes of a one dimensional photonic crystal

$$E(x.t) = E_k(x,t) = u_k(x)e^{i(kx-\omega_k t)} \qquad (3.4).$$

Eq. 3.4 tells us that each eigenmode is characterized by a wave vector k. ω_k denotes the eigen-frequency and $u_k(x) = u_k(x + a)$ is the periodic Bloch function. Hence $E_k(x, t)$ is periodic and expanding in a Fourier series results in

$$E_k(x,t) = \sum_{m=-\infty}^{\infty} E_m e^{i\left(k+\frac{2\pi m}{a}\right)x - i\omega_k t} \qquad (3.5).$$

We can assume for simplicity that only components with m = 0, ±1 are dominant in the expansion of $\varepsilon_r(x)$:

$$\varepsilon_r^{-1}(x) \approx k_0 + k_1 e^{i\frac{2\pi}{a}x} + k_{-1} e^{-i\frac{2\pi}{a}x} \qquad (3.6).$$

The problem is solved if we substitute eq. 3.5 and 3.6 into the wave equation 3.2. Here we skip the details of calculation (see for a complete treatment Ref. 47) and we will discuss the results. The eigen-frequencies are:

$$\omega_{\pm} \approx \frac{\pi c}{a}\sqrt{k_0 \pm |k_1|} \pm \frac{ac}{\pi|k_1|}\left(k_0^2 - \frac{|k_1|^2}{2}\right)\left(k - \frac{k}{a}\right)^2 \qquad (3.7)$$

as far as $(k - \pi/a)^2 << \pi/a$, there is no mode in the interval

$$\frac{\pi c}{a}\sqrt{k_0 - |k_1|} < \omega < \frac{\pi c}{a}\sqrt{k_0 + |k_1|} \qquad (3.8).$$

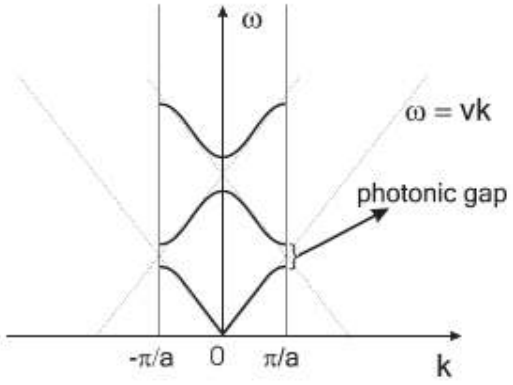

Figure 3.2: Dispersion relation for a 1D photonic crystal in the first Brillouin zone (solid curve), compared with the dispersion relation for a homogeneous material $\omega = vk$ (dashed lines). When the two dispersion lines cross, they repel each other and a photonic gap appears.

This photonic gap disappears only if $k_1 = 0$. This result can be interpreted as due to the coupling of the modes with $k \approx \pi/a$ and $k \approx -\pi/a$ in the presence of the periodic modulation of the dielectric constant and this mixing leads to a frequency splitting. The resulting band diagram is depicted in Figure 3.2, where the dispersion relation for the 1D photonic crystal is compared with the dispersion for a homogeneous material.

For a semiconductor the treatment is very similar. Starting from the Schrödinger equation for an electron in a periodic potential $V(x) = V(x + a)$,

$$\left[\frac{p^2}{2m} + V(x)\right]\psi(x) = E_0\psi(x) \qquad (3.9),$$

where $\psi(x)$ is the wave function of the electron and E_0 is the energy eigenvalue, we obtain a similar solution for the dispersion relation as in the photonic case. If now we consider the waves equation 3.2 in its scalar form and we assume that it has solutions of the type $E(x, t) = E(x)\, e^{(i\omega t)}$, we have:

$$\frac{\partial^2 E(x)}{\partial x^2} + \varepsilon_r(x)\left(\frac{\omega}{c}\right)^2 E(x) = 0 \qquad (3.10).$$

Rewriting Eq. 3.10, we obtain

$$-\frac{\partial^2 E(x)}{\partial x^2} + \left(\frac{\omega}{c}\right)^2 (1-\varepsilon_r(x))E(x) = \left(\frac{\omega}{c}\right)^2 E(x) \qquad (3.11).$$

We can now define a *light potential* $V_{light}(x, \omega) = (\omega/c)^2(1 - \varepsilon_r(x))$, so that for photons we have

$$-\frac{\partial^2 E(x)}{\partial x^2} + V_{light}(x,\omega)E(x) = \left(\frac{\omega}{c}\right)^2 E(x) \qquad (3.12),$$

which is very similar to the Schrödinger equation:

$$-\frac{\hbar^2}{2m}\frac{\partial^2 \psi(x)}{\partial x^2} + V(x)\psi(x) = E_0\psi(x) \qquad (3.13).$$

We can now make a comparison between the wave equation 3.12 and the Schrödinger equation 3.13. The differences are only due to the potentials:

- When $\varepsilon_r(x) = 1$ (vacuum), $V_{light} = 0$. This is valid immediately outside the sample. In contrast the Coulomb potential V has a finite range for a finite piece of material, also outside the sample.
- For propagating waves $\varepsilon_r(x) \geq 1$ (excluding left handed materials, that are not treated in this thesis), which means that the difference $(\omega/c)^2 - V_{light}$ is always positive. This means that bound states for light do not exist, while for electrons the difference can be both positive or negative: one can have valence and conduction electrons.
- $V_{light}(x,\omega)$ depends on the energy and it vanishes for low values of ω; in other words for small frequencies the material becomes more and more transparent.

The band diagram and the comparison between waves and Schrödinger equations was made in one dimension, but similar considerations hold in two and three dimensions. The photonic band gap forms because of the periodicity of the refractive index, similar to the formation of the electronic bandgap in a semiconductor.
Photonic crystals can be one-, two- and three-dimensional and several fabrication strategies have been developed to make such structures. In this dissertation, we focused on one dimensional photonic structures, that are the most common ones to make a laser resonator (or cavity).

3.3. 1D vertical diffractive resonators

A key class of resonator for organic semiconductor lasers are diffractive structures. These resonators do not use either mirrors or total internal reflection for feedback, but instead use periodic, wavelength-scale microstructures that

diffract, or Bragg-scatter the light (Figure 2.6e-f). These periodic structures can be readily incorporated into planar organic semiconductor waveguides and avoid the need for good-quality end facets to provide the feedback. By imposing a periodic surface corrugation on the organic semiconductor film, one may create a structure that will reflect propagating waveguide modes without needing to form end facets. There have been many different diffractive structures explored for organic semiconductor lasers, including simple diffraction gratings that form so-called distributed feedback (DFB) lasers, two- and three-dimensional photonic crystal structures, and concentric circular gratings that provide a radial feedback about a particular point. There have also been lasers with *a*periodic feedback structures based on high-rotational-symmetry photonic quasi-crystals [48-51], or even with completely random scattering centres that may provide closed-loop feedback in the films [52-70]. Distributed feedback lasers have proved particularly successful [36,38,71-86] and are discussed herein.

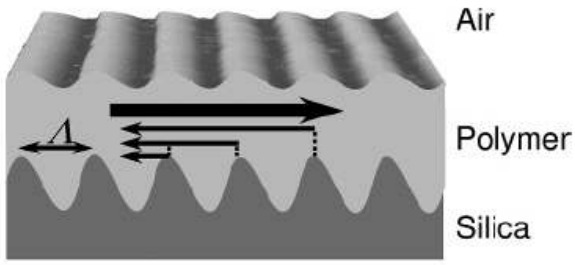

Figure 3.3: Schematic structure of a polymer DFB laser with corrugations of period λ. Light of wavelength $\lambda = 2\, n_{eff} \Lambda$ propagating from left to right is scattered from the periodic structure to create a diffracted wave propagating in the counter-propagating waveguide mode.

Figure 3.3 shows a typical structure of a polymer DFB laser with diffractive feedback along one axis in the plane of the waveguide. The laser consists of a

thin organic semiconductor film deposited on top of a corrugated fused silica substrate. Light propagating in a waveguide mode of the high-index organic film is scattered by the periodic corrugations. The scattered light from each corrugation combines coherently to create a "Bragg-scattered" wave propagating in some new direction. The angle through which the light is Bragg-scattered, or diffracted, is highly wavelength dependent, so one finds that different wavelengths are diffracted into different directions. For a given period of the corrugation, there is a particular set of wavelengths that will be diffracted from a propagating mode of the waveguide into the counter-propagating waveguide mode. This situation will arise when the Bragg condition is satisfied:

$$m\lambda = 2\, n_{eff}\Lambda \tag{3.14}$$

Here, λ is the wavelength of the light, Λ is the period of the structure, and m is an integer that represents the order of the diffraction. n_{eff} is the so-called effective refractive index of the waveguide; this is a geometrical average of the refractive indices of the three layers of the waveguide and may be calculated through a solution of the Helmholtz wave equation for a planar multilayer structure. For first-order diffraction therefore the wavelength of the reflected light will equal twice $n_{eff}\Lambda$. For the case of $m = 2$, the reflected wavelength is equal to $n_{eff}\Lambda$, but now light is also diffracted out of the surface of the film perpendicular to the plane of the waveguide. Such second-order structures can therefore provide a surface-emitted output coupling of the laser light via first-order diffraction while providing in-plane feedback via second-order diffraction.

The full theory of DFB lasers is somewhat more complicated than this simple diffractive picture, since the wavelength that exactly satisfies the Bragg condition cannot propagate in the film. This leads to what is known as a

photonic stopband, centred on the Bragg wavelength, for light propagating in a direction perpendicular to the grating grooves (discussed in the previous sections). This behaviour is described by the coupled mode theory of Kogelnik and Shank that predicts that the DFB laser will normally oscillate on a pair of wavelengths, one at either edge of this photonic stopband [12-14].

The spacing between these wavelengths is determined by the strength of the diffractive coupling of the counter-propagating waves. Thus this diffractive structure has an advantage over the Fabry-Perot lasers in that it provides both a long resonator length in which the optical field can interact with the gain medium (and hence give a low oscillation threshold), and strong spectral selection of the resonant light. DFB lasers based on inorganic semiconductors are commonly used in telecommunication applications, taking advantage of the stable spectral output for multiplexing many wavelength channels together [11].

3.4. Modelling

The photonic structures that are used as diffractive resonators to make a DFB laser can be modelled by using several mathematical instruments. MIT Photonic Bandgap MIT Photonic Bandgap (MPB) [87], that is a GNU licence software developed by S. G. Johnson, calculates the band structure of the periodic dielectric structure. The inputs for the calculation are the refractive index of the two materials and the ratio between their thicknesses (d_{PVK}/d_{CA}). The program assumes that the periodic structure has infinite number of layers and the layers have infinite area.

Comsol Multiphysics is a commercially available software that solves numerically second order differential equations. The geometry is the multilayer of the two materilas. For the calculation, we have used scalar equation for the

transverse electric field component E_Z $-\nabla \cdot \nabla E_z - n^2 k_0^2 E_z = 0$, where n is the refractive index and k_0 is the free space wave number [43,88].

3.5. Sensing Applications

The concept of a *responsive* photonic crystal has been developed for the first time in 1996 [89]. In that case, a switchable three-dimensional photonic crystal was created, by combaining crystalline colloidal array self-assembly of monodisperse polystyrene spheres with the temperature-induced volume phase transition of poly(N-isopropylacrylamide) (PNIPAM). Briefly, they dispersed the polystyrene spheres in an aqueous solution containing NIPAM monomer; the polystyrene spheres self-assembled in a bcc lattice. Then they photochemically initiated NIPAM polymerization to create a polystyrene photonic crystal embedded in a PNIPAM hydrogel. The obtained composite film shrinks and swells continuously and reversibly between 10°C and 35°C.

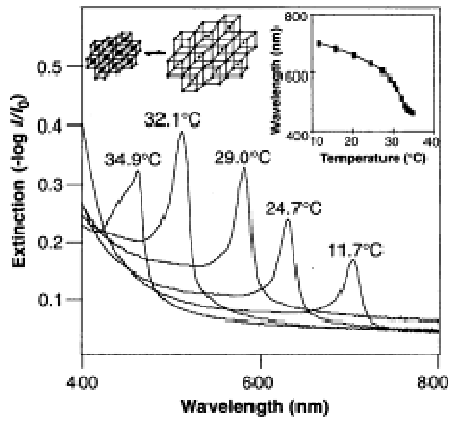

Figure 3.4: Temperature tuning of Bragg diffraction from a 125-μm-thick PCCA film of 99-nm PS spheres embedded in a PNIPAM gel. The shift of the diffraction wavelength results from the temperature-induced volume change of the gel, which alters the lattice spacing. Spectra were recorded in a UV-visible-near IR

spectrophotometer with the sample placed normal to the incident light beam. The inset shows the temperature dependence of the diffracted wavelength for this PCCA film when the incident light is normal to the (110) plane of the lattice.

In Figure 3.4 it is shown that, decreasing the temperature, the periodicity of the photonic lattice increases and, consequently, the photonic band gap exhibits a bathochromic effect.

After this work, in the literature there are a lot of examples of sensors based on photonic crystals [90-100]. Among the photonic crystals, the one-dimensional, especially the multilayer geometry, are the ones that have shown the best performances. In 2007, the group of Prof. Edwin L. Thomas proposed a one dimensional photonic crystal made with polyelectroactive polymers (known to be highly responsive to a range of stimuli) that shows very large reversible optical changes due to variation of the salt concentration of a water reservoir where the photonic crystal is immersed. These one-dimensional Bragg stacks reflect incident light from the ultraviolet–visible region to the near-infrared region λ_{peak} = 350 – 1.600 nm) with over a 575 % change in the position of the stop band [101].

Polystyrene-b-quaternized poly(2-vinyl pyridine) (PS-b-QP2VP) is a hydrophobic block–hydrophilic polyelectrolyte block polymer that swells and shrinks due to salt concentration, consequently changing the optical path of the multilayer (Fig. 3.5) [102].

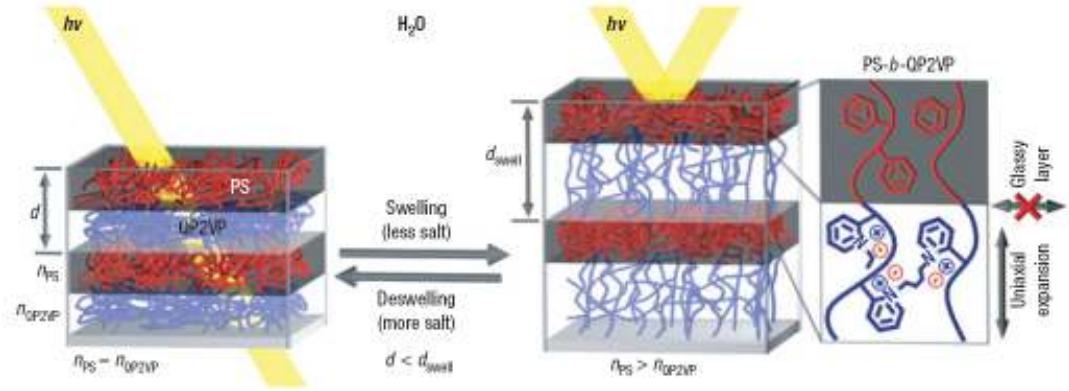

Figure 3.5: Schematic diagram of the structure of photonic gel film and the tuning mechanism. The photonic gel film was prepared by self-assembly of a diblock copolymer (PS-b-QP2VP). Swelling/deswelling of the QP2VP gel layers (blue) by aqueous solvents modulates both the domain spacing and the refractive-index contrast, and accordingly shifts the wavelengths of light (hv) reflected by the stop band. The hydrophobic and glassy polystyrene layers (red) limit expansion of the gel layers to the direction normal to the layers.

The concept of a DFB laser sensor was reported by the group of Prof. Bulovic in 2005. In that case, the threshold was very sensitive to DNT and TNT exposure: After the exposure to this analyte, the laser peak did not occur, i.e. the threshold increased [103].

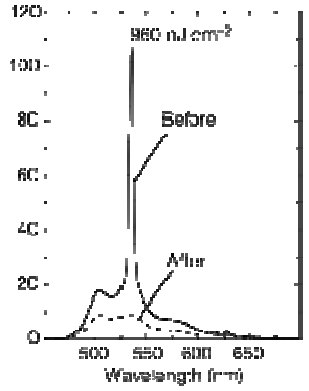

Figure 3.6: Emission of the DFB laser before and after exposure to DNT [103].

Chapter 4
Experimental section

4.1. Materials

4.1.1. Gain Materials

We have used two gain materials for our experiments. The first is a purchased molecule, Rhodamine 6G, while the second is a synthesised polymer, poly (phenylene vinylene). In Figure 4.1 the chemical structures of the two materials are shown.

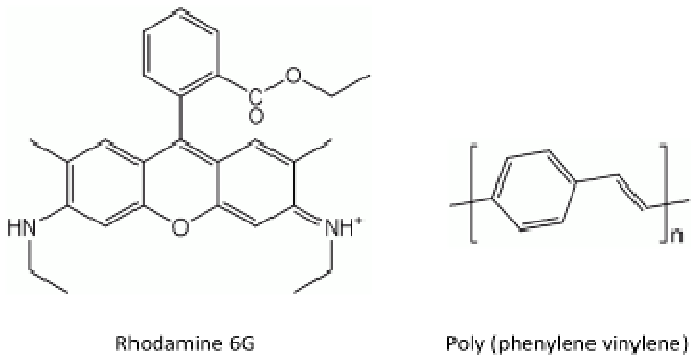

Figure 4.1: Chemical structures of Rhodamine 6G and Poly (phenylene vinylene).

The absorption and emission spectra of Rhodamine 6G (R6G, purchased by Acros Organics) are shown in Figure 4.2. The absorption maximum is around 530 nm with a very large molar extinction coefficient (116000 M^{-1} cm^{-1}, Ref. 104). The fluorescence emission shows a maximum at 570 nm. The Fluorescence quantum yield of the molecule is 0.86 at room temperature [105]. R6G is soluble in water and in many polar solvents. To prevent aggregation

quenching, in the solid state, it is useful to disperse the molecule in a polymer matrix.

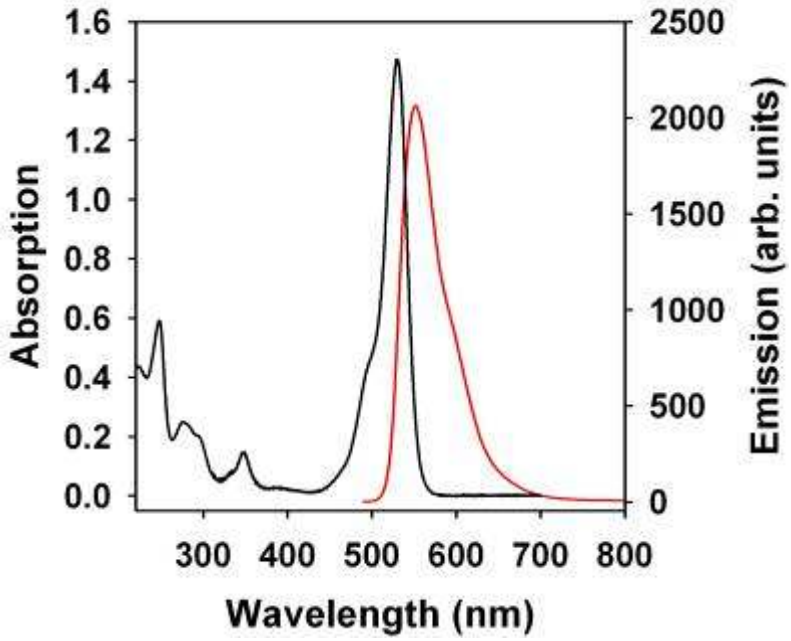

Fig. 4.2: Absorption and emission spectra of Rhodamine 6G.

Poly (phenylene vinylene) has a maximum of his absorption at about 400 nm and the maximum of the emission at 540 nm (Fig. 4.3). The luminescence quantum yield is 0.22 [106].

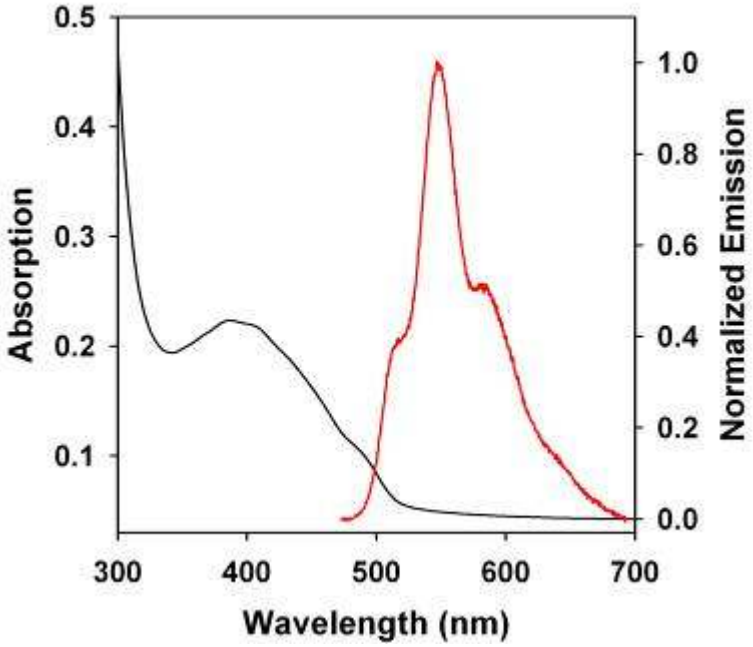

Figure 4.3: Absorption and emission spectra of PPV.

In literature there are many reports on the demonstration of stimulated emission with R6G and PPV. Then, they are very suitable for laser action and good candidates as active media in DFB lasers.

4.1.2. Materials for photonic crystals

To make a one dimensional photonic crystal, we have deposited with a spin coater (see below) alternated layers of materials (sequence ABABAB…). For our works, two types of one dimensional photonic crystal are made: polymeric and nanoparticle-based photonic crystals. The polymers used are poly vinylcarbazole (PVK) and cellulose acetate (CA). Their chemical structures are shown in Figure 4.4.

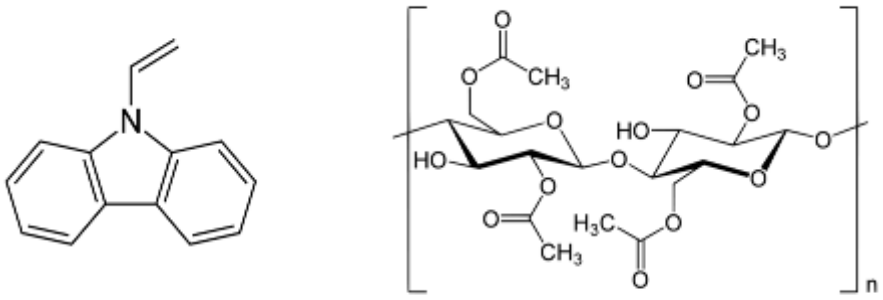

Figure 4.4: Chemical structures of PVK and CA.

Although PVK is a polymer that can exhibits spontaneous emission (it has an absoption maximum at about 350 nm and emits at 400 nm), we do not use this polymer as active material. Instead, we take advantage of its high refractive index (1.683, Ref. 107) by using it as a material constituting the photonic crystal. To make a polymer solution with PVK, we dissolve it in chlorobenzene. PVK (and chlorobenzene) is purchased by Acros Organics and possesses an average molecular weight of 90000. CA is a transparent polymer (up to 200 nm) and has a refractive index of 1.475 [107]. It is soluble in diacetone alcohol (both are purchased by Acros Organics) and its average molecular weight is 100000. For the polymeric photonic crystals we have used ethanol washed glass slides as substrates.

The two types of nanoparticles we have used are made with Silicon dioxide (SiO_2) and Titanium dioxide (TiO_2). SiO_2 nanoparticles were purchased from Aldrich (Ludox SM-30). TiO_2 nanoparticles used in this work were prepared according to literature protocol [108]. Briefly, titanium ethoxide was added dropwise to 0.1M HNO_3 at room temperature under vigorous stirring. The suspension was then peptized by stirring at 80°C for 8hrs. The resulting

dispersion was filtered to remove any agglomerates and subsequently diluted to the desired concentration.

For these photonic crystals we have used Piranha and air-plasma treated glass slides and silicon wafers as substrates. Prior to spin-coating (see below the spin coating paragraph) each dispersion was stirred thoroughly, sonicated for 10 mins and filtered through a 0.45 μm pore syringe filter to remove any aggregates. Following each bilayer deposition, the SiO_2/TiO_2, nanoparticle DBRs were thermally treated at 450^{o}C for 30 min.

4.2. Spin coating

The spin coating is an experimental technique to deposit uniform thin films on flat (in rarely case also on curve) substrates.

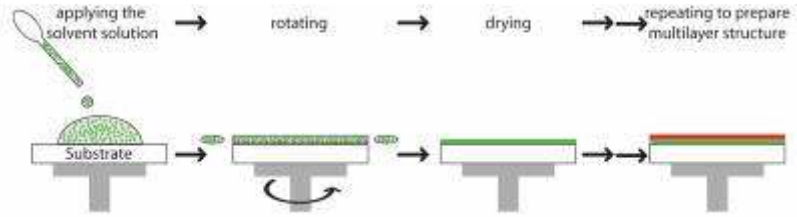

Figure 4.5: Spin coating procedure.

The procedure is schematically shown in Figure 4.5. An excess amount of solution is placed on the substrate which is then rotated at high speed in order to spread the fluid by centrifugal force.

Rotation is continued while the fluid spins off the edges of the substrate, until the desired thickness of the film is achieved. The applied solvent is usually volatile, and simultaneously evaporates. So, the higher the angular speed of spinning, the thinner the film. The thickness of the film also depends on the concentration of the solution and the solvent. [109]

4.3. Transmission and reflection spectra

Transmission spectra in the range 200 to 800 nm were collected using a Varian Cary 50 (bandwidth 1 nm). Reflectance spectra in the range 350 to 850 nm were collected using an Ocean Optics SD2000 fiber–optic diode–array dual–channel spectrometer interfaced with an ocular tube of an Olympus BX41 binocular microscope by fibre optics, using the microscope's light source (Olympus TH4–100) and a 20x working distance objective (Olympus 20X/0.40 BD LMPlan FI). HRSEM was performed using a Hitachi S–5200 (10 – 15 kV, 15 mA).

4.4. Laser measurements

For the lasing measurements (setup in Figure 4.6), the light source we used a Nd:YAG pulsed laser (Quanta System). The emission wavelength of this laser is 1064 nm, corresponding to the Nd^{3+} ion transition $^4F_{3/2} \rightarrow {}^4I_{11/2}$. The pulse duration is 5 nanoseconds and the repetition rate can be tuned between 1 and 10 Hz. For our measurements, we used a repetition rate of 1 Hz. By using two optically non-linear crystals for Second Harmonic Generation (SHG) we can generate the second and the fourth harmonic, 532 and 266 nm, respectively (we used 532 nm). The non-linear crystals are KH_2PO_4, usually named KDP [110].
Spectra have been recorded with two types of detector: a nitrogen cooled CCD (Spex 2000) coupled to a polychromator (Triax 190 from J-Horiba), with a bandpass of 0.2 nm for signal detection, and a mini-spectrometer Hamamatsu C10083MD coupled to an optical fiber with a sensitivity between 320 and 1000 nm and a bandpass of 2 nm.
Excitation laser light has been removed by using a proper notch filter (Edmund Optics).

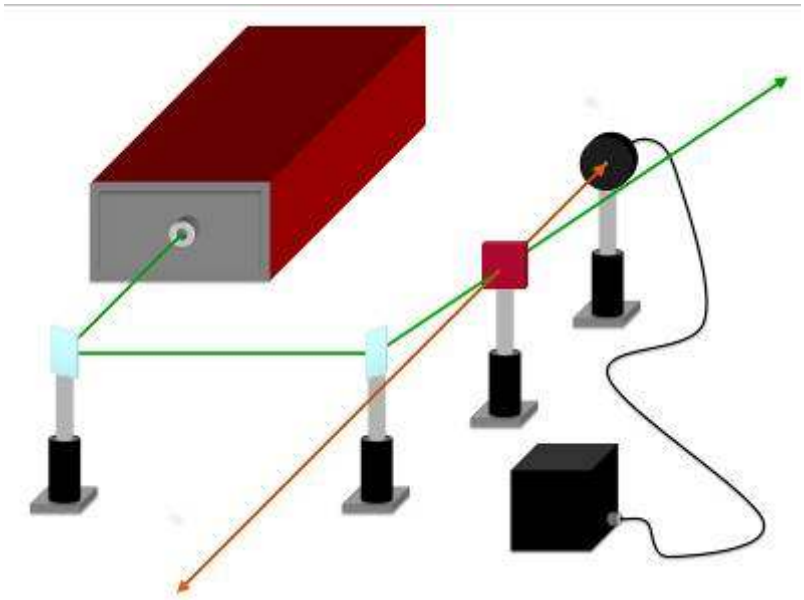

Figure 4.6: Laser measurement setup.

4.5. SEM and Confocal Microscopy

For a morphological characterization of nanoparticle-based one dimensional photonic crystals we used the instrumentation at the Center of Nanostructure Imaging (CNI), a facility of the Department of Chemistry, University of Toronto.

The Scanning Electron Microscope we used is a Hitachi S-5200. The resolution of this microscope depends on the applied working voltage: 0.4 nm at 30 kV, 1.8 nm at 1 kV. A unique detector enables both secondary electrons (SE) and backscattered electrons (BSE) imaging.

The laser confocal microscope is a Leica TCS SP2. It is equipped with lenses 20x, 50x, 63x and 80x and with several lasers: an Ar^+ ion laser (50 mW) with wavelength at 458, 476, 488 and 514 nm, a green HeNe laser (1.2 mW) at 543 nm and a red HeNe laser (10 mW) at 633 nm.

To take an image (SEM or confocal) of a one dimensional photonic crystal cross section, we cut the photonic crystal fabricated on a silicon substrate (by using a glass the focusing of the electron beam on the sample is cumbersome) and we put the sample in order to have the electron beam normal to the cross section.

Chapter 5
Results and Discussion

In this section we will present the different types of fabricated DFB lasers. In this way, we treat each DFB laser by showing its structural and morphological properties and its laser characteristics, analyzing and discussing the performance and the limits.

5.1. Polymeric Photonic Crystals for DFB lasers

5.1.1. DFB lasers on glass substrates

In order to predict the photonic structure which we want to fabricate with the two polymers (PVK and CA), we have calculated the band structure with MIT Photonic Bandgap. The inputs for this calculation are the refractive indexes of the two materials and the ratio between their thicknesses. The used script is:

```
(define-param n-lo 1.475)
(define-param n-hi 1.683)
(define-param w-hi (/ 1 4))
;ratio between the layers thicknesses
(set! geometry-lattice (make lattice (size 1 no-size no-size)))
(set! default-material (make dielectric (index n-lo)))
(set! geometry (list (make cylinder (material (make dielectric
 (index n-hi))) (center 0 0 0) (axis 1 0 0) (radius infinity)
(height w-hi))))
…
(set! k-points (interpolate 60 k-points))
(set-param! resolution 32)
```

```
(set-param! num-bands 8)
(run-te)
; note that TM and TE bands are degenerate, so we only need TE
```

The program assumes that the structure is infinite in all directions. In Figure 5.1a the calculated dispersion relation, and the corresponding photonic density of states, is depicted. The photonic density of states is high in proximity of the photonic band edges, while is suppressed over the range of the band gap. The photonic band gap is narrow and this is due to the relatively low refractive index contrast of the two polymers (~ 1.14). Nevertheless, for a DFB laser application, this phenomenon is negligible while the zero group velocity at the photonic band edge is the main feature. With Comsol Multiphysics we have numerically calculated (by solving second-order differential equations) the propagation of an electromagnetic wave (λ = 600 nm). Figure 5.1b shows that the electromagnetic wave is completely reflected when it passes through a 39-layers 1D PC.

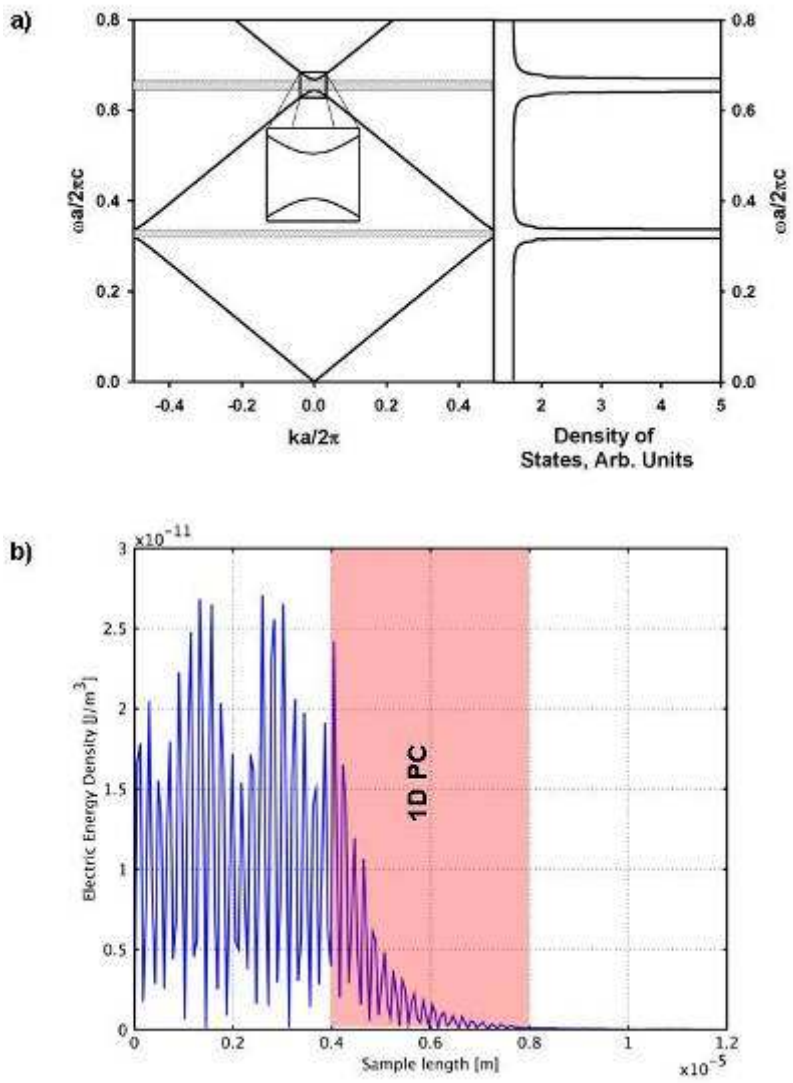

Fig. 5.1: a) dispersion relation and photonic density of states of a PVK/CA multilayer; b) propagation of a 600 nm electromagnetic wave in a 39-layer PVK/CA multilayer (the sample is depicted with a red rectangle).

We have fabricated a photonic crystal made by 19 layers of alternated PVK and CA (doped with R6G, 0.5 wt %). In Figure 5.2a the transmission spectrum is shown. The photonic band gap is centred at about 600 nm, with the blue edge at 585 nm, and the absorption of the dye shows the peak at 530 nm. The other

peak at 400 nm is the second order of the photonic band gap. Fig. 5.2b shows the trend of the transmission spectrum of the dye-doped 1D PC versus the incident angle of light θ. In the range between 520 and 540 nm, the absorption of R6G is shown, and it, obviously, does not change, whereas the photonic band gap, the higher order photonic band gap, shows a blue shift of the order of 150 nm. The higher order PBG shows a blue shift toward the region of PVK absorption. This is because the position of the photonic band gap follows the Bragg Snall law:

$$m\lambda_{Bragg} = 2D\sqrt{n_{eff}^2 - \sin^2\theta} \qquad (5.1)$$

where m is the diffraction order, λ_{Bragg} is the wavelength where the photonic band gap is centred, n_{eff} is the effective refractive index, D is the unit cell of the photonic crystal and θ is the incidence angle measured off from the normal.

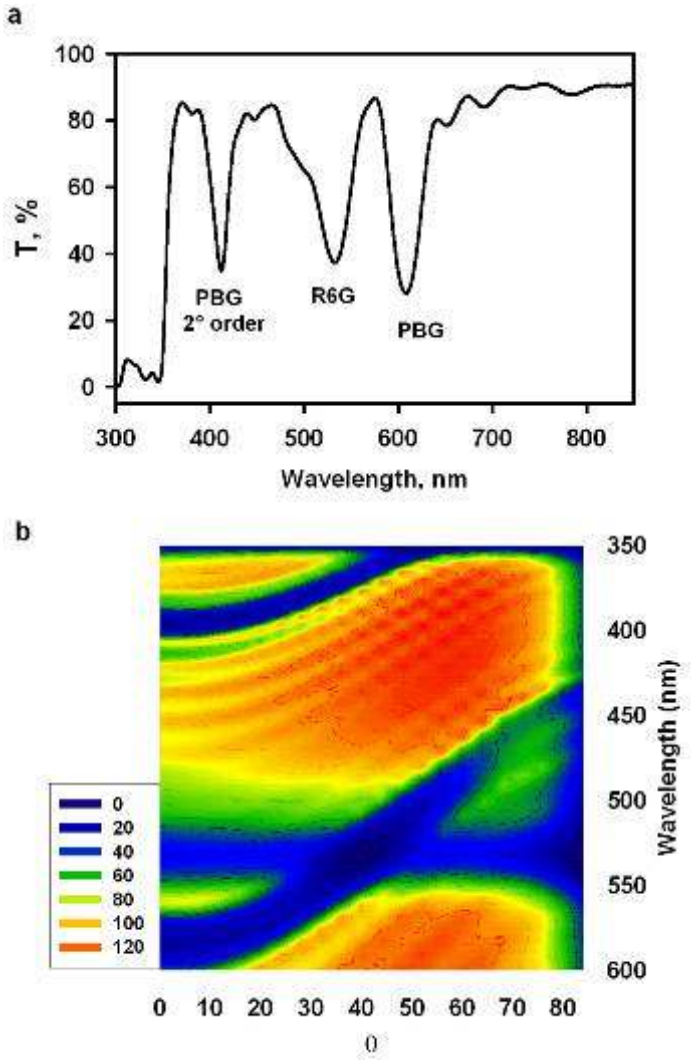

Fig. 5.2: a) Transmission spectrum and b) transmission spectrum versus the incident angle of light of a fabricated 19-layer PVK/CA multilayer.

In Figure 5.3a the photoluminescence spectra of the R6G-doped 1D PC, at different pump energy density, are reported. The photoluminescence signal has been revealed normally to the surface of the multilayer.

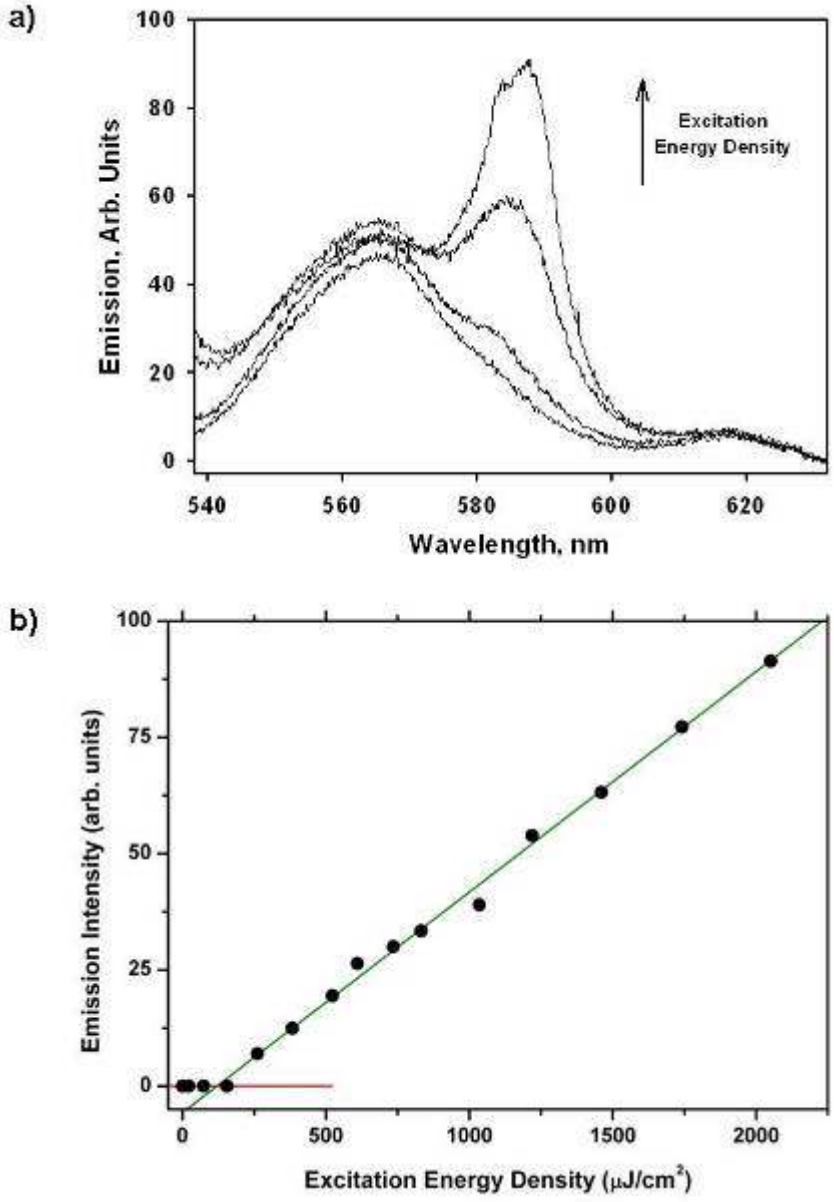

Fig. 5.3: a) Photoluminescence at different excitation energy densities and b) laser characteristics of the dye-doped polymeric DFB laser.

The region between 540 and 570nm shows the luminescence peaks of the dye, while between 570 and 630nm remarkable effects arise from the superimposition of the luminescence of the dye with the photonic structure. In

the range of energy where the photonic band gap is present, the luminescence of the dye is suppressed, while, at the energy corresponding to the first (higher energy) photonic band edge, the emission of the dye exhibits a narrow peak arising from the enhancement of the emission in the region of the high density of states. A typical signature of the laser action is displayed in Fig. 5.3b: the input-output characteristics (excitation energy density versus output emission intensity) with a threshold followed by a linear increase of the emission intensity [32]. For this system the value of the threshold is set at about 120 $\mu J/cm^2$ [111].

5.1.2. DFB Lasers on flexible substrates

By using polymeric and organic materials there are some fabrication advantages, as as the possibility of depositing on large-area and flexible substrates. Thus, we prepared polyvinylcarbazole and cellulose acetate (doped with R6G, 0.5 wt %) solution and we spin coated on a cellulose substrate 19 layers alternating the two polymers.

Figure 5.4a shows the ratio v_g/c calculated by Eq. 1 (purple line, v_g is the group velocity). The thickness parameters have been optimized in order to have one of the photonic band edges in correspondence of R6G gain region. The selected couple of calculated thicknesses is a = 45 nm and b = 140 nm. Figure 5.4b reports the transmission spectrum of the sample FML (green line), fabricated by following these indications. Several structures can be observed: a first transmission minimum appears at 570 nm. This PBG overlaps the absorption peak of R6G at 532 nm. The narrow peak at 380 nm is the second order PBG: since the refractive index changes with the wavelength, the experimental 2^{nd} order PBG is at lower energies in respect to its theoretical position at 285 nm obtained by considering n_2 and n_1 as constants.

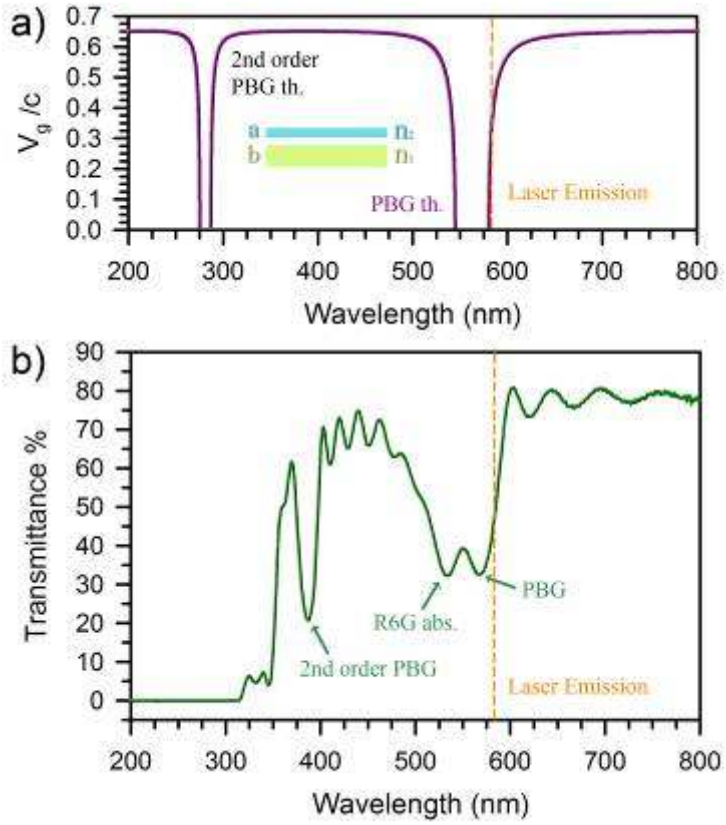

Fig. 5.4: a) Computed group velocity in the 1D periodic structure as function of the wavelength of traveling photons with a = 45 nm, b = 140 nm, n_2= 1.683 and n_1= 1.475. b) Transmission spectrum of FML sample taken at normal incidence.

To analyze the effect of the photonic structure on the lasing emission, sample luminescence has been studied as a function of the incident power density. Emission spectra showed in Figure 5.5 have been detected by exciting the sample at 2.33 eV (532 nm) by the second harmonic of a pulsed Nd:YAG solid state laser. The pump laser impinged on the sample obliquely with respect to the normal incidence. At low exciting power density, the sample shows the broad photoluminescence band (Figure 5.5a, blue line), corresponding to the dye emission only slightly shaped by the PBG. By increasing the exciting

power per pulse, a peak appears at 580 nm, completely dominating the broad emission when a power density of ~ 50 mJ/cm^2 is used (Figure 5.5a, orange line). The weak peak at 532 nm is due to pumping laser emission, not completely reflected by the notch filter. Figure 5.5b shows the integrated emission intensity of the FML sample in the range of investigated excitation energy densities. When the sharp peak starts to be detectable, we observe an abrupt increase of the overall PL intensity, thus highlighting the threshold of the lasing emission; the PL enhancement appears exactly at the energy corresponding to the lowest group velocity v_g as predicted by the model previously proposed. The threshold power density has been estimated to be ~ 17 mJ/cm^2, corresponding to the onset of the change of the PL intensity: this value is almost one order of magnitude lower than the power density required to have laser emission in R6G doped polymeric matrix [112], as expected from our calculation. The threshold is followed by a linear increase of the emission and a line narrowing, both signatures of laser action [32]. The full width at half maximum (FWHM) of the peak is about 15 nm, which is a relatively large value even though similar FWHM values for DFB structures are reported in the literature [103]. The corresponding quality factor of the lasing cavity is Q ~ 40. This value, low for a DFB laser, can be ascribed to the number of bilayers (unit cells) constituting our structure, smaller than the typical number of repeating unit in grating based systems [80]. Furthermore, the laser peak is the convolution of the lasing emissions from slightly different band edges due to the small non-homogeneity of our photonic 1D crystal. Figure 2c shows the emission intensity as a function of the angle of detection φ (φ = 0 when the detection is normal to the sample surface, along the dielectric periodicity): the intensity is the highest when φ = 0 as expected from the coherence characteristics of a lasing emission.

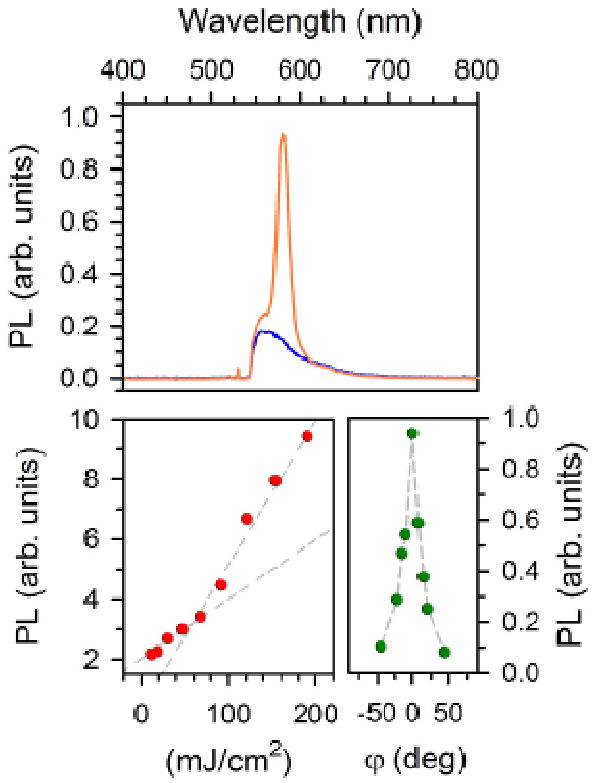

Fig. 5.5: a) FML emission spectrum at excitation power density of 50 mJ/cm^2 (orange line) and of 5 mJ/cm^2 (blue line). The peak at 532 nm is due to excitation laser stray-light. b) Overall FML luminescence intensity as function of the incident power density. c) Over threshold emission intensity as a function of the angle of detection φ ($\varphi = 0$ when the detection is normal to the sample surface, along the dielectric periodicity).

The picture reported in Figure 5.6 shows one of the most intriguing characteristics of our laser, which has been fabricated on a flexible cellulose substrate and so can be easily bent. This device is very stable in term of laser peak position, despite any sort of bending. As shown in Figure 5.6, we didn't observe any substantial difference in the laser peak position and width (blue line for the flat sample, red line for the bent sample) The behaviour suggests that the variation of the thickness induced by the stretching is negligible [113].

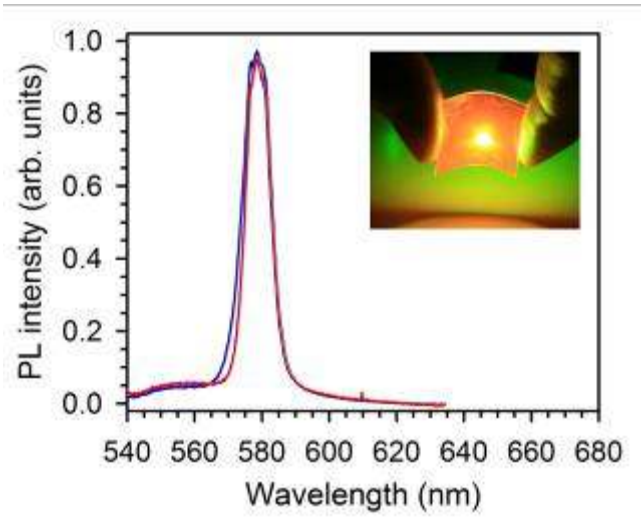

Fig. 5.6: Over threshold emission for the flat (blue line) and the bended flexible DFB laser (red line). Inset: picture of the flexible DFB laser.

5.2. Nanoparticle 1D Photonic Crystal Dye Laser

The photonic crystal, a representative example of which is shown in the SEM of Figure 5.7a, consists of 22 periodically alternating layers of SiO_2 and TiO_2 prepared by sequential spin-coating of the appropriate SiO_2 and TiO_2 nanoparticle aqueous dispersions. The effective refractive index of the SiO_2 layers and the TiO_2 layers were determined by spectroscopic ellipsometry to be 1.21 and 1.80 at 598 nm respectively. From the effective refractive indices as well as layer thicknesses, the porosities of the SiO_2 and TiO_2 layers were determined to be 38% and 34% respectively. The gain material (R6G) was absorbed into the photonic structure by immersing the PC in a 10^{-3} M R6G water solution for 24 hours.

A cross-sectional confocal optical microscopy image is provided in Figure 5.7b effectively demonstrating that the dye uniformly permeates the entire photonic

structure. The limited spatial resolution of confocal optical microscopy does not allow the distribution of dye within the SiO_2 and TiO_2 layers to be elucidated. Nevertheless, it should be emphasized that the porosity of the nanoparticle 1D PC along with the coulombic interaction between the nanoparticles of the PC and the dye are key features of this system as such enables uptake of a large quantity of dye which in turn provides the opportunity of creating a lasing architecture made from a self-assembled nanoparticle-based 1D PC.

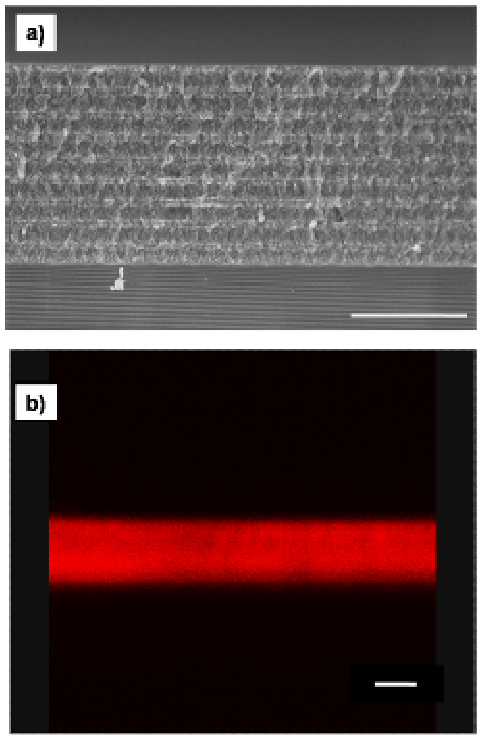

Fig. 5.7: a) SEM cross section image of a SiO_2/TiO_2 nanoparticle 1D PC (scale bar = 1μm); b) confocal microscopy image of the dye-loaded nanoparticle 1D PC (scale bar = 1.5μm). Note that the thicknesses of the images correlate well.

To establish the theoretical basis for the work described herein, the properties of a one dimensional photonic structure bearing the aforementioned optical features were predicted by solving the corresponding transfer matrix [114].

Figure 2a shows the calculated transmission spectrum of a finite 1D photonic structure, consisting of 11 layers of SiO_2 alternating with 11 layers of TiO_2, with thicknesses of 145 and 65 nm, respectively (such values are approximations to the actual thicknesses employed). The most notable feature of the transmission spectrum is the presence of a broad photonic stopband which represents the range of photon frequencies that cannot propagate in the 1D PC. From the transmission spectrum it is also possible to derive the photonic density of states (Fig 2b) of such a 1D photonic structure, which most importantly for the work described herein, is high at both the red and blue edges of the photonic stopband, and consequently tends to zero over the range of the stopband frequencies.

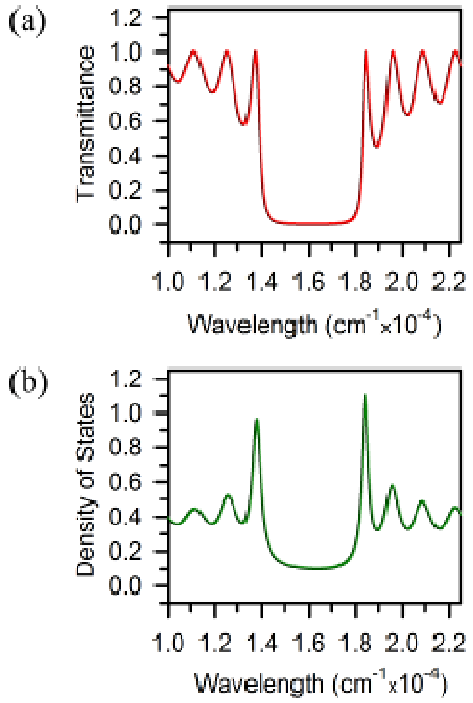

Fig. 5.8: a) Calculated transmission spectrum of 11 layers of nanoparticle SiO_2 and nanoparticle TiO_2 solving the transfer matrix; b) calculated photonic density of states

(DOS) of the structure and (c) distribution of the photonic density of states along the layers.

The experimental reflectance spectrum of the SiO_2/TiO_2 1D PC infiltrated with R6G is provided in Figure 5.9b, (blue line). It displays a high reflectivity broad band from 550 to 650 nm, with a maximum at about 600 nm, thus corresponding to predicted minimum of transmittance (Figure 5.8a). This effect could be entirely ascribed to the periodicity of the dielectric lattice which generates a photonic stopgap.

The optical setup used to acquire photoluminescence measurements is described in detail in the experimental section. For such measurements, the pulsed second harmonic of a Nd^{3+} doped yttrium aluminum garnet laser was employed as the pump with a repetition rate of 1 Hz and with a pulse width of 5 ns. As showed in Figure 5.9a, the pump laser light impinges on the sample obliquely with respect to normal incidence. The resulting emission is vertical in respect to the sample surface, most notably in the direction parallel to the dielectric periodicity.

The pulse energy density used in our experiments was always maintained at a value an order of magnitude below the destruction of the sample (0.6 J/cm^2): the pump beam was focused onto a spot with an area of about 1 mm^2 and all luminescence measurements were carried out under ambient conditions. Laser light has been carefully removed by using a proper notch filter.

By exciting the sample with a pump energy density of 40 $\mu J/cm^2$, a narrow emission peak (Figure 3b, orange line) is clearly detectable at about 548 nm (~18250 cm^{-1}) corresponding to the energy where the blue edge of the photonic stopband overlaps the R6G spontaneous emission, which is depicted in Figure 5.9a. This is in relatively good agreement with the theoretical predictions where a maximum of the DOS is predicted (Figure 5.8b), around 544 nm (18400 cm^{-}

[1]). In addition and again as predicted by each of the calculations of Figure 5.8, it is important to note that almost all dye emission beyond 548 nm is suppressed owing to the presence of the photonic stopband. The observation of such phenomena effectively establishes that the stimulated emission at 548 nm is associated with the DFB structure, a result of the coupling of the emission of R6G with the blue band-edge of the nanoparticle 1D PC.

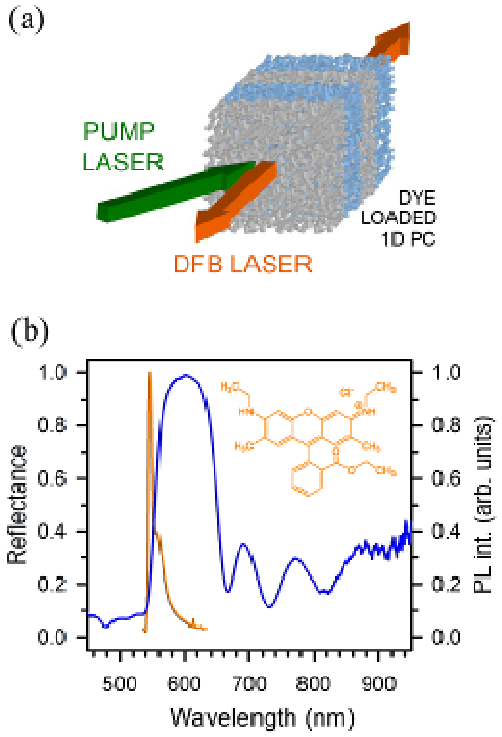

Fig. 5.9: a) Schematic representation of the sample; b) experimental reflectance spectrum (blue line) and photoluminescence (orange line) of the dye loaded nanoparticle 1D PC excited by pulsed laser light at 532 nm with a energy density of 40 μJ/cm^2. The inset shows the molecular structure of the R6G dye.

Inset of Figure 5.10a shows the overall intensity of the photoluminescence of the sample has been studied as a function of the incident laser excitation energy density over a range of 6 to 40 μJ/cm^2. Increasing the excitation energy density,

we observed an abrupt change in the photoluminescence intensity concomitant with the rise of the peak at 548 nm. The corresponding onset energy density upon which the aforementioned phenomena of increased emission intensity appears can be considered as the lasing threshold of the system; it was determined to be approximately 12 $\mu J/cm^2$. It is worth mentioning here that such a threshold is one of the lowest reported for a bottom-up nanofabricated laser device**.** Figure 5.10a shows representative luminescence spectra of the sample below (blue line) and above (purple line) the threshold power. The emission above the threshold has been collected by using neutral optical filters on the signal detection in order to reduce the intensity. The photoluminescence spectrum below threshold shows the broadband emission of the organic dye, which is slightly modified by following the photonic band gap profile. However, once the sample is excited above the threshold excitation power we obtain a narrow emission of about 8 nm FWHM, corresponding to a cavity quality factor Q ~ 70. The observation of this phenomenon establishes that the stimulated emission at 548 nm can be associated with the DFB structure created by the 1D PC. As expected, the amplified luminescence emission takes places strictly at energies corresponding to the spectral regions with high density of allowed photonic states, which are only determined from the intrinsic properties of the periodic dielectric structure [14,19,115].

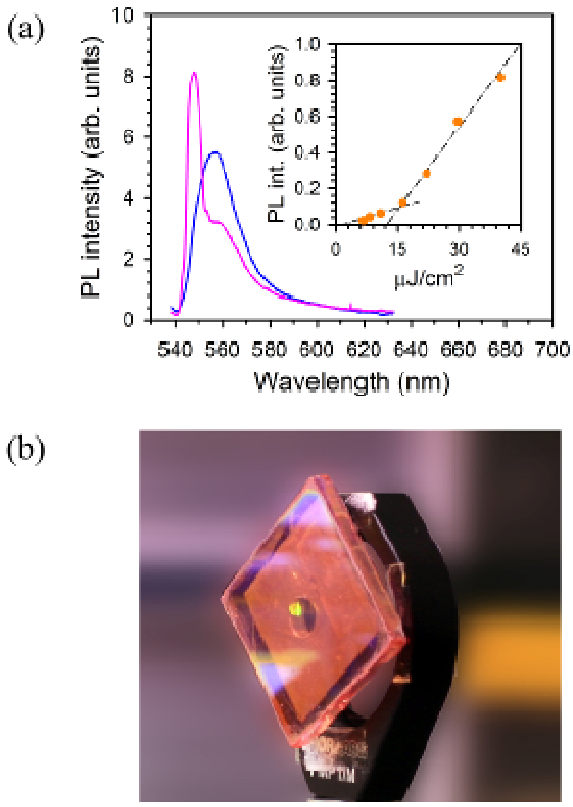

Fig. 5.10. a) Photoluminescence spectra of the sample below (blue line) and above (purple line) the lasing threshold. Inset: overall PL intensity as a function of the excitation energy density at 532 nm. The threshold energy density is about 12 μJ/cm^2; b) image of the sample excited by pulsed laser light at 532 nm with an energy density of 40 μJ/cm^2.

5.3. DFB Laser from a Composite PPV-Nanoparticle 1D PC

A photonic crystal made with the same fabrication method of chapter 1.3 (22 periodically alternating layers of nanoparticle SiO_2 and TiO_2), precursor PPV, prepared by the synthetic scheme provided in Figure 5.11, was drop-cast or spin-cast onto the photonic crystal in order to effectively infiltrate the pores of the latter. Nevertheless, regardless of the method of PPV infiltration, an

undesired polymer overlayer was always present which was easily removed by gently scraping the overlayer with a glass slide. Here the polymer is easily removed as it is significantly softer than the polymer/NP composite and thus the latter remains intact suffering minimal degradation. Once the PC is infiltrated and the overlayer removed, the precursor was thermally converted to the desired conjugated structure by heating at 225^{o}C for 3 hrs. under N_2 [116]. A cross-sectional confocal optical microscopy image is provided in Figure 5.12b effectively demonstrating that the polymer uniformly permeates the entire photonic structure which is of course again made possible by the mesoporosity of the nanoparticle 1D PC. It is the porosity of such a structure that truly enables the inclusion of the emitting polymer into the pores which in turn ultimately affords the capability of fabricating a composite emitting polymer/NP 1D PC laser. The photograph of Figure 5.12c, which is of the PPV/NP 1D PC composite under UV excitation is a true testament to the aforementioned attributes.

a)

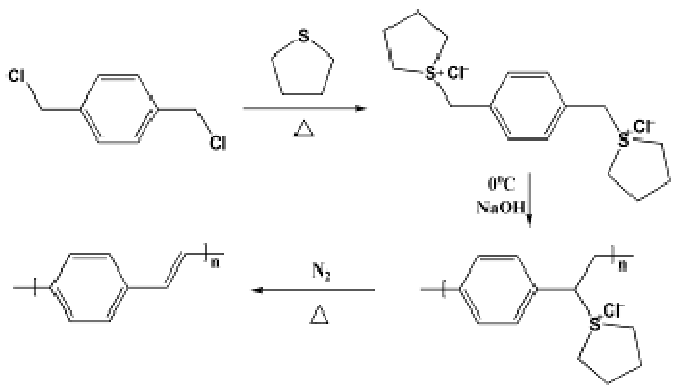

b)

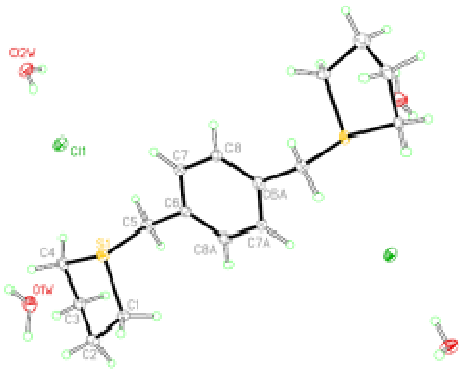

Fig. 5.11. a) Synthetic scheme employed for the synthesis of PPV. b) The molecular structure of the monomer to the polyelectrolyte PPV precursor, p-xylene-bis(tetrahydrothiophenium chloride), with displacement ellipdoids drawn at the 30% probability level [117-120].

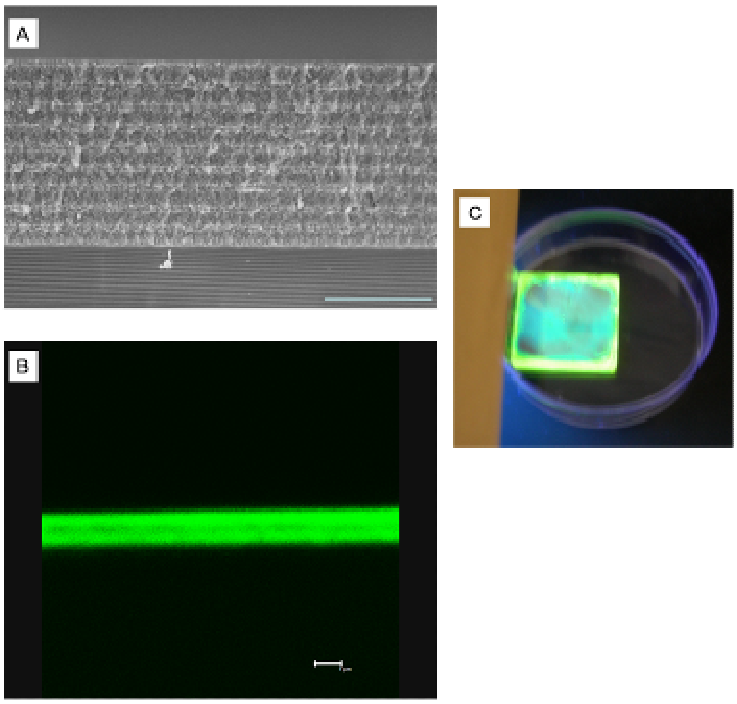

Figure 5.12: a) SEM of an 11-bilayer SiO_2/TiO_2 nanoparticle Bragg reflector (scale bar = 1 µm). b) A cross-sectional confocal microscopy image of the PPV infiltrated NP 1D

PC (scale bar = 1 μm), note that the thickness correlates well with the thickness of the SEM in a). c) Photograph of the PPV/NP 1D PC composite under UV excitation.

The absorption and spontaneous emission spectrum of a pure 300nm thick PPV film is shown in Figure 4.3. The absorption has a maximum ~400nm and thus this wavelength was selected as the pump wavelength. The spontaneous emission of the thermally converted polymer is broad extending over a range of 500-690nm which is indeed advantageous for this application as it imposes severe restrictions on the position of the 1D PC Bragg reflectance. The reflectance spectrum of a PPV infiltrated NP 1D PC is shown in Figure 5.13a (black line). The broad band between 530 and 630 nm, with a peak reflectance at 570 nm corresponds to the photonic stopgap of the NP 1D PC. A comparison of reflectance and the spontaneous emission reveal a significant overlap, which is of course a pre-requisite for the development of the desired band edge laser.

The optical setup used to acquire photoluminescence measurements is described in detail in the experimental section. For such measurements, the DFB was pumped by 100 fs pulses at 400 nm at a repetition rate of 1 kHz, obtained from the second harmonic of a Ti:Sapphire amplified laser. The beam, incident at an angle of ~20 degrees to the surface normal, was focused on a circular excitation area (1.1×10^{-4} cm^2) and the emission was measured with an optical multichannel analyzer (OMA, 1.2 nm resolution).

As mentioned previously, the spontaneous emission of PPV exhibited good overlap with the Bragg peak of the constructed 1D PC. The function of the PC in this application is a modulation of the photon density of states (DOS) of the composite. In this 1D PC system, the DOS is high at the band edges and tends to zero in the bandgap. Thus, for an emitting species confined within the NP PC, provided that there exists good overlap (as is the case in our system) with the emission of the emitter and the Bragg peak of the DBR, it is expected that

emission wavelengths overlapping the band edges will be enhanced and those overlapping the stopgap will be suppressed. At high enough excitation energy density, the gain within the system should exceed the losses and lasing be observed. It is worth noting that the ideal system would be one whereby the blue edge of the stopgap of the NP PC exactly overlaps the gain maximum of the emitting polymer. Such a system is very challenging to construct however owing to the difficulty in precision controlling of the stopgap position as well as the sensitivity of the polymer conjugation length (and thus the gain spectrum) on the fabrication conditions. Nevertheless, although the aforementioned condition certainly represents the ideal, it's realization is not absolutely necessary to obtain stimulated emission as we achieved this situation by simply ensuring sufficient overlap of polymer emission with the blue edge of the PC. As shown in Figure 5.13a, above an excitation energy density of 550 $\mu J/cm^2$, a narrow peak (FWHM ~3 nm) centered at 520 nm can be observed. The observed lasing wavelength correlates well with the blue edge of the PC stopgap and thus the vertical DFB photonic structure provides an efficient feedback to light inside the cavity.

In Figure 5.13b we plot the input-output (i.e. excitation energy – output intensity) characteristics of the emission. It shows the typical signatures of laser action: a clear threshold at approximately 100 nJ, with concomitant line narrowing (from ~40 to ~3 nm) and a linear increase for higher excitation energies. Note that the linear increase is obtained over a very large range of input energies (from 100 to 1400 nJ) which is worth emphasizing as this effect is seldom achieved with organic lasers as usually saturation and degradation play a major role at higher excitation conditions. The threshold corresponds to an energy density of 550 $\mu J/cm^2$, of absorbed light, as the exciting laser beam is focused on an area of 1.1×10^{-4} cm^2, This value is in good agreement with thresholds for other organic DFB lasers reported in literature [84]. It is expected

that the threshold can be lowered by increasing the number of layers of the DFB structure as this would augment the feedback mechanism [121].

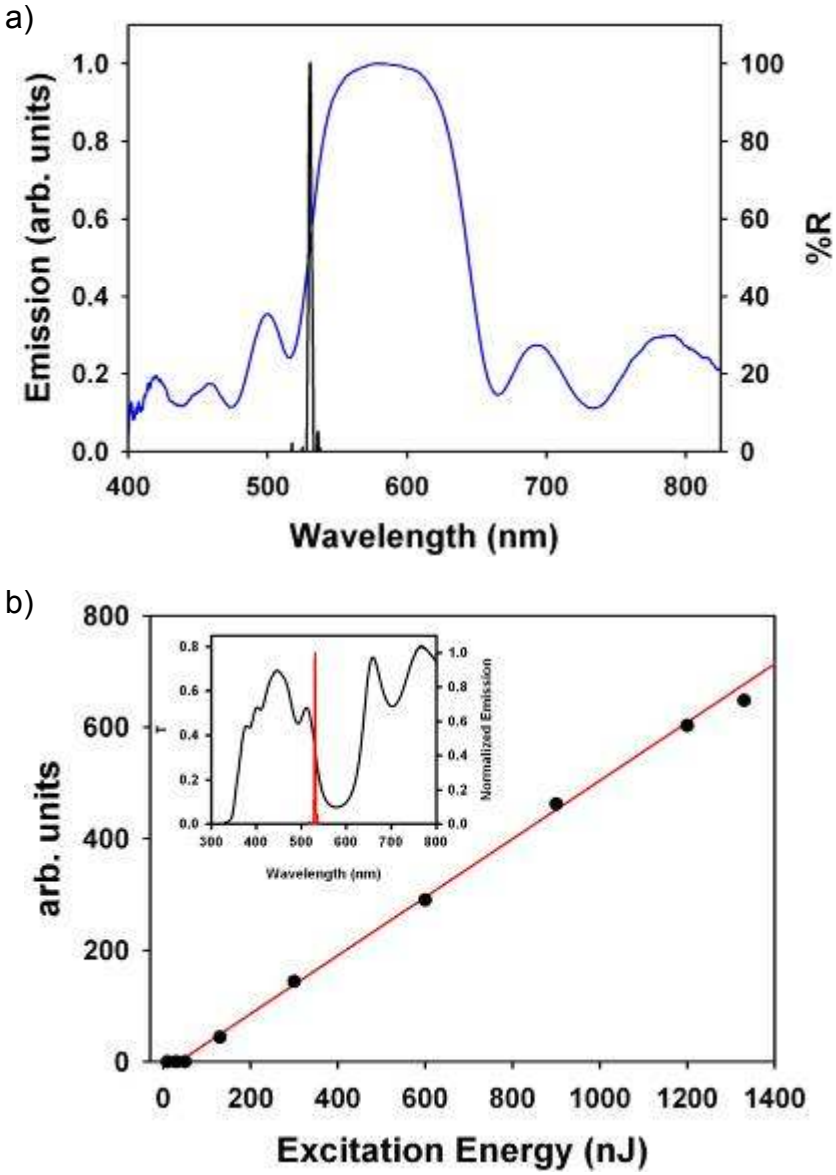

Fig. 5.13. a) Reflectance spectrum of a PPV infiltrated NP 1D PC (blue) along with the emission spectrum of the composite above threshold; b) Input-output (i.e. excitation energy – output intensity) characteristics of the emission of the composite. Inset:

transmission spectrum of the NP 1D PC (black line) and laser peak of the PPV infiltrated NP 1D PC.

Chapter 6
Conclusion

6.1. Overview on the Fabricated DFB Lasers

We have fabricated and characterized four different types of DFB lasers: all-organic DFB laser on rigid and flexible substrates, a nanoparticle-based DFB dye laser and a composite poly (phenylene vinylene)-Nanoparticle DFB laser. We have demonstrated stimulated emission for all the systems, through the input-output characteristics. Nevertheless, the sample shows different behaviour, above all the laser threshold. The lowest threshold, in terms of excitation energy density, has been achieved with the nanoparticle 1D photonic crystal dye laser (subsection 1.3), and we ascribed this phenomenon to the high optical quality of the fabricated photonic crystal that can be observable in Fig. 5.7. The same type of photonic crystal has been used for the composite PPV/nanoparticle DFB laser, but the threshold in this case is 550 $\mu J/cm^2$, but we should underline that we have used different experimental conditions, as the pump source, 400 nm instead of 532 nm, its repetition rate and pulse duration, 1 kHz and 100 fs instead of 1 Hz and 5 ns. Moreover, the PPV we have synthesised has a quantum yield of 22%, while the quantum yield of the laser dye is 0.86, and this difference drives to diverse laser dynamics.

An extension of the work would involve the development a dye doped NP based microcavity (consisting of periodically alternating layers of SiO_2 and TiO_2 nanoparticles with a central SiO_2 NP defect layer) [122]. It is expected that the lasing performance of the analogous microcavity will be superior to that described here as the DOS of the cavity mode greatly exceeds the DOS at the band edges.

6.2. Environmental Sensing with 1D PC: a Step Towards DFB Laser Sensor

One dimensional photonic crystals, fabricated by multilayer deposition, possess a fundamental advantage: in principle, the materials constituting the layers can be any kind of molecule, polymer or inorganic compound. In Figure 6.1 the SEM cross sections of different photonic crystal structures are shown. In this case, nanoparticles made by Silicon dioxide, Titanium dioxide, Laponite (clays), Silicalite (Zeolite) nanoparticles, Tin dioxide and Antimonium doped Tin dioxide. The size of these nanoparticles is between 15 and 50 nanometers. Other materials as mesoporous Silicon dioxide and Titanium dioxide are interesting for one dimensional photonic crystals. Moreover, nanoparticles can be functionalised with several molecules as, for example, any type of silanes (easily the Silicon atom in the silane reacts with the Oxigen atoms at the surface of the nanoparticles) [16].

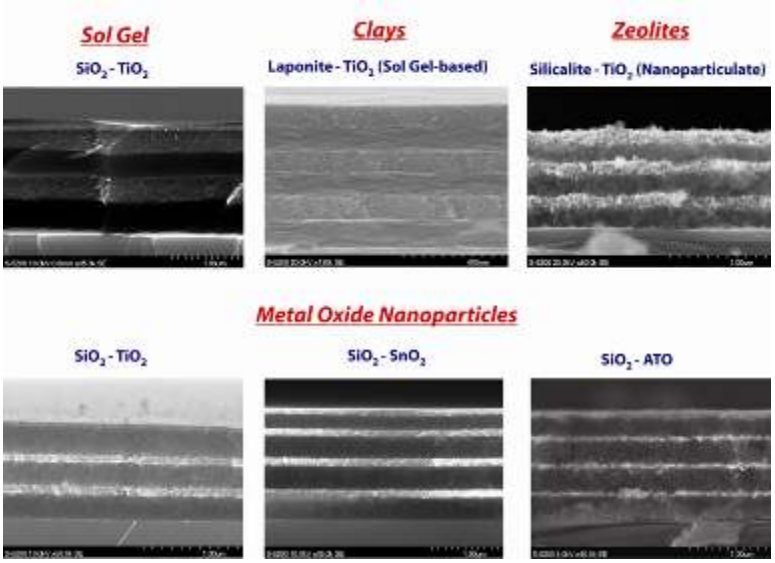

Fig. 6.1: SEM images of different photonic crystal structures with the materials constituting the repeating unit indicated above each image.

An interesting property of these nanoparticle-based photonic crystals is that they change their optical thickness when specific liquids or vapours percolate within the nanoparticle intra-pores. By changing the optical thickness of the photonic crystal, the position of the corresponding photonic band gap shift the lower energies (with a directly observable change of the reflected colour). This property is very useful for different applications, above all the environmental sensing.

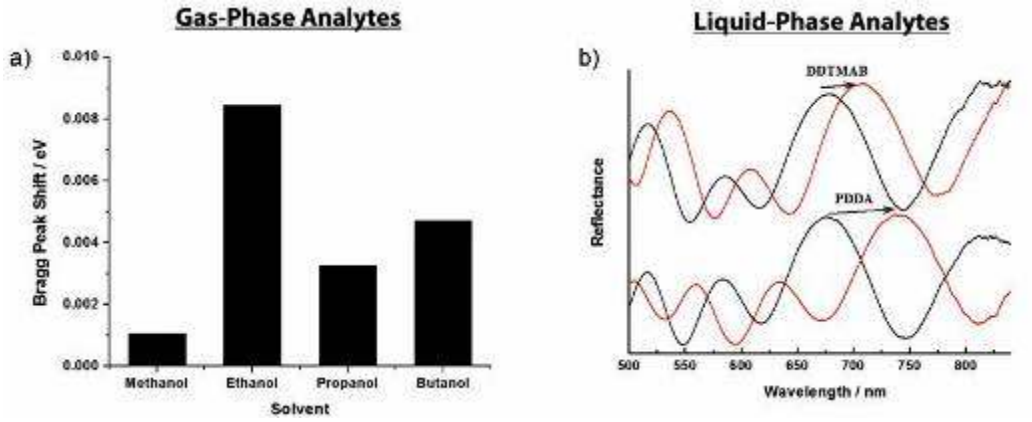

Fig. 6.2: a) Photonic band gap shift magnitude upon exposure of a 4-bilayer SiO_2/SnO_2 photonic crystal to different solvent vapour atmospheres; a) Solution phase analyte uptake from a Laponite-mesoporous TiO_2 photonic crystal (DDTMAB = Dodecyltrimethylammonium Bromide; PDDA = Poly(diallyldimethylammonium chloride) (PDDA).

In Figure 6.2a the shift magnitude (in eV) of the photonic band gap upon exposure of a silane-functionalised nanoparticle SiO_2/SnO_2 photonic crystal to different solvent vapour atmospheres is shown. The shift of the PBG is selective to the different vapour: due to the hydrophobic surface of the silane-

functionalised nanoparticles senses more small alcohols than water. Also, sensors for liquid-phase analyte have been fabricated by using Laponite and mesoporous TiO_2, which senses more PDDA that DDTMAB (Figure 6.2b), with a shift of photonic bandgap position of almost 100 nm. A 100 nm shift means a clearly observable colour change, for example from the green to the red (from 500 to 600 nm). The sensing properties of these porous photonic crystals can be tailored by using diverse molecules to functionalise the nanoparticle surface in order to selectively sense only specific analytes, e.g. air and water pollutants.

A logical extension of this work is the estimation of the limit of detection (LOD), for a better understanding of the sensitivity of the sensor. An interesting way to enhance the LOD is the infiltration in the photonic crystals of an appropriate laser dye or polymer emitter, which overlaps its emission with one of the edges of the photonic bandgap, in order to make a DFB laser. The shift of the photonic bandgap, due to the presence of a critical concentration of pollutant, provokes the shift of the edges of the photonic bandgap, consequently changing the lasing threshold (the edge moves to another region of the dye/polymer emission with a different intensity) or even switching off the laser emission.

Publications and Contributions

The work and the studies during the developement of the thesis provided the publication of the following papers, and the following contributions to international conferences and meetings.

Journal Papers:

[J-1] **F. Scotognella**, A. Monguzzi, F. Meinardi, R. Tubino, *DFB laser action in a flexible fully plastic multilayer*, Physical Chemistry Chemical Physics, *accepted*

[J-2] D. P. Puzzo, **F. Scotognella**, M. Zavelani-Rossi, M. Sebastian, A. J. Lough, I. Manners, G. Lanzani, R. Tubino, G. A. Ozin, *Distributed Feedback Lasing from a Composite Poly(Phenylene Vinylene)-Nanoparticle One-Dimensional Photonic Crystal*, Nano Letters, 10.1021/nl902516t (2009)

[J-3] G. A. Ozin, K. Hou, B. V. Lotsch, L. Cademartiri, D. P. Puzzo, **F. Scotognella**, A. Ghadimi, J. Thomson, *Nanofabrication by self-assembly*, Materials Today, 12(5), 12 (2009)

[J-4] **F. Scotognella**, D. P. Puzzo, A. Monguzzi, D. S. Wiersma, D. Maschke, R. Tubino, G. A. Ozin, *Nanoparticle 1D Photonic Crystal Dye Laser*, Small, 5(18), 2048 (2009)

[J-5] L. Cademartiri, **F. Scotognella**, P. G. O'Brien, B. V. Lotsch, N. P. Kherani, G. A. Ozin, *Crosslinking ultrathin nanowires: A platform for nanostructure formation and biomolecule detection*, Nano Letters, 9(4), 1482 (2009)

[J-6] **F. Scotognella**, F. Meinardi, M. Ottonelli, L. Raimondo, R. Tubino, *Judd-Ofelt analysis of a novel Europium organic complex*, Journal of Luminescence, 129, 746 (2009)

[J-7] L. D. Bonifacio, B. V. Lotsch, D. P. Puzzo, **F. Scotognella**, G. A. Ozin, *Stacking*
the Nanochemistry Deck: Structural Diversity in One-Dimensional Photonic
Structures, Advanced Materials, 21(16), 1547 (2009)

[J-8] A. Monguzzi, J. Mezyc, **F. Scotognella**, R. Tubino, F. Meinardi, *Upconversion-induced fluorescence in multicomponent systems: steady-state excitation power threshold*, Physical Review B, 78, 195112 (2008)

[J-9] **F. Scotognella**, A. Monguzzi, M. Cucini, F. Meinardi, D. Comoretto, R. Tubino, *One dimensional polymeric organic photonic crystals for DFB lasers,* International Journal of Photoenergy (2008)

Refereed Conference Presentations:

[C-1] National Conference "XCV Congresso Nazionale, Società Italiana di Fisica" (Bari, September 28 – October 3 2009). Contribution: oral Contribution. Title: *Fully Organic Multilayer DFB lasers*.

[C-2] European School on Chemistry and Physics of Materials for Energetics (Milano, September 14-19 2009). Contribution: poster presentation. Title: *One Dimensional Photonic Crystal DFB Lasers for Photonic and Sensing Applications*.

[C-3] Workshop on "Bio-Inspired Photonic Structures" (Donostia-San Sebastian, July 9 – 15 2009). Contribution: oral presentation.

[C-4] National Conference "VI Convegno nazionale materiali molecolari avanzati per fotonica ed elettronica" (Arbatax, June 24 – 27 2009). Contribution: oral presentation.

[C-5] International Conference "European Optical Society Annual Meeting 2008" (Paris, September 28 – October 2 2008). Contribution: poster presentation.

[C-6] International Conference "SOLAR '08 International Conference on Molecular/Nano-Photochemistry" (Il Cairo, Egypt, March 24-28 2008). Contribution: keynote oral presentation.

[C-7] International Conference "ECOER 2007 4th European Conference on Organic Electronics and Related Phenomena" (Varenna (LC), October 1-4 2007). Contribution: poster presentation.

[C-8] PhD school "Mesoscopic structures, dynamics and optics" in collaboration with the "European Doctorate in Physics and Chemistry of Advanced Materials" (August 6–14 2007, Alsion – Sonderborg, DENMARK). Contribution: oral presentation.

Refereed Conference Presentations (as coauthors):

[C-9] L. D. Bonifacio, B. V Lotsch, D. P Puzzo, F. Scotognella, G. A Ozin, *Piling Nanomaterials: Functional One-Dimensional Photonic Crystals*, MRS Spring Meeting, (San Francisco, CA, April 13-17 2009). Contribution: poster presentation.

[C-10] A. Monguzzi, F. Meinardi, R. Tubino, J. Mezyk, F. Scotognella, *Non-Coherent Ultra Loe Power Up-Conversion in Multicomponent Organic Systems*, MRS Fall 2008 (December 1-5 2009, Boston, USA). Contribution: oral presentation.

[C-11] A. Monguzzi, F. Scotognella, R. Tubino, F. Meinardi, *Low power upconversion-induced delayed fluorescence: kinetics considerations and exchange interactions role*, International Conference "SOLAR '08 International Conference on Molecular/Nano-Photochemistry" (Il Cairo, Egypt, March 24-28 2008). Contribution: oral presentation.

References

[1] R. S. Quimby, *Photonics and Laser*, John Wiley & Sons, Inc., Hoboken, New Jersey, **2006**;

[2] J. Hecht, *Understanding Lasers*, 3rd Ed., John Wiley & Sons, Inc., Hoboken, New Jersey, **2008**;

[3] http://nobelprize.org/;

[4] B. H. Soffer, B. B. McFarland, *Appl. Phys. Lett.* **1967**, *10*, 266;

[5] N. Karl, Phys. Status Solidi A **1972**, 13, 651;

[6] O. S. Avanesjan, V. A. Benderskii, V. K. Brikenstein, V. L. Broude, L. I. Korshunov, A. G. Lavrushko, I. I. Tartakovskii, *Mol. Cryst. Liq. Cryst.* **1974**, *29*, 165;

[7] Moses D., *Appl. Phys. Lett.* **1992**, 60, 3215;

[8] N. Tessler, G. J. Denton, R. H. Friend, *Nature* **1996**, 382, 695;

[9] S. John, *Phys. Rev. Lett.* **1987**, 58, 2486;

[10] E. Yablonovitch, *Phys. Rev. Lett.* **1987**, 58, 2059;

[11] I. D. W. Samuel, G. A. Turnbull, *Chem. Rev.* **2007**, 107, 1272;

[12] H. Kogelnik, C. V. Shank, *Appl. Phys. Lett.* **1971**, *18*, 152;

[13] H. Kogelnik, C. V. Shank, *J. Appl. Phys.* **1972**, *43*, 2327;

[14] J. P. Dowling, M. Scalora, M. J. Bloemer, C. M. Bowden, *J. Appl. Phys.* **1994**, *75*, 1896;

[15] M. Salerno, G. Gigli, M. Zavelani-Rossi, S. Perissinotto, G. Lanzani, *Appl. Phys. Lett.* **2007**, 90, 111110;

[16] L. D. Bonifacio, B. V. Lotsch, D. P. Puzzo, F. Scotognella, G. A. Ozin, *Adv. Mater.* **2009**, 21, 1641;

[17] S. Colodrero, M. Ocana, H. Miguez, *Langmuir* **2008**, 24, 4430;

[18] D. P. Puzzo, L. D. Bonifacio, J. Oreopoulos, C. M. Yip, I. Manners, G. A. Ozin, *J. Mat. Chem.* 2009, 19, 3500;

[19] F. Scotognella, D. P. Puzzo, A. Monguzzi, D. S. Wiersma, D. Maschke, R. Tubino, G. A. Ozin, *Small* **2009**, 5, 2048;

[20] C. W. Tang; S. A. Vanslyke, *Appl. Phys. Lett.* **1987**, 51, 913;

[21] Frolov, S. V.; Ozaki, M.; Gellermann, W.; Vardeny, Z. V.; Yoshino, K. *Jpn. J. Appl. Phys., Part 2* **1996**, 35, L1371;

[22] Denton, G. J.; Tessler, N.; Stevens, M. A.; Friend, R. H. *Adv. Mater.* **1997**, 9, 547;

[23] G. Heliotis, R. Xia, D. D. C. Bradley, G. A. Turnbull, I. D. W. Samuel, P. Andrew, W. L. Barnes, *Appl. Phys. Lett.* 2003, 83, 2118;

[24] G. Heliotis, D. D. C. Bradley, G. A. Turnbull, I. D. W. Samuel, *Appl. Phys. Lett.* **2002**, 81, 415;

[25] J. R. Lawrence, G. A. Turnbull, I. D. W. Samuel, G. J. Richards, P. L. Burn, *Opt. Lett.* **2004**, 29, 869;

[26] S. Yokoyama, A. Otomo, S. Mashiko, *Appl. Phys. Lett.* **2002**, 80, 7;

[27] A. Otomo, S. Yokoyama, T. Nakahama, S. Mashiko, *Appl. Phys. Lett.* **2000**, 77, 3881;

[28] T. Spehr, A. Siebert, T. Fuhrmann-Lieker, J. Salbeck, T. Rabe, T. Riedl, H. H. Johannes, W. Kowalsky, J. Wang, T. Weimann, P. Hinze, *Appl. Phys. Lett.* **2005**, 87, 161103;

[29] R. Xia, G. Heliotis, M. Campoy-Quiles, P. N. Stavrinou, D. D. C. Bradley, D. Vak, D. Y. Kim, *J. Appl. Phys.* **2005**, 98, 083101;

[30] T. Spehr, R. Pudzich, T. Fuhrmann, J. Salbeck, *Org. Electron.* **2003**, 4, 61;

[31] N. Johansson, J. Salbeck, J. Bauer, F. Weissortel, P. Broms, A. Andersson, W. R. Salaneck, *Adv. Mater.* **1998**, 10, 1136;

[32] A. E. Siegman, *Lasers*, University Science Books, Sausalito, CA, **1986**;

[33] O. Svelto, *Principles of Lasers*, 4th ed., Plenum Press, New York, **1998**;

[34] A. I. Rudenko, H. Bassler, *Chem. Phys. Lett.* **1991**, 182, 581;

[35] V. G. Kozlov, V. Bulovic, P. E. Burrows, S. R. Forrest, *Nature* **1997**, 389, 362;

[36] R. Gupta, M. Stevenson, A. J. Heeger, *J. Appl. Phys.* **2002**, 92, 4874;

[37] H. J. Brouwer, V. V. Krasnikov, A. Hilberer, J. Wildeman, G. Hadziioannou, *Appl. Phys. Lett.* **1995**, 66, 3404;

[38] T. Rabe, M. Hoping, D. Schneider, E. Becker, H. H. Johannes, W. Kowalsky, T. Weimann, J. Wang, P. Hinze, B. S. Nehls, U. Scherf, T. Farrell, T. Riedl, *Adv. Funct. Mater.* **2005**, 15, 1188;

[39] K. L. Shaklee, R. F. Leheny, *Appl. Phys. Lett.* **1971**, 18, 475;

[40] N. de la Rosa-Fox, *Opt. Mater.* **1999**, 12, 267;

[41] M. Berggren, A. Dodabalapur, R. E. Slusher, Z. Bao, *Nature* **1997**, 389, 466;

[42] M. D. McGehee, R. Gupta, S. Veenstra, E. K. Miller, M. A. Diaz-Garcia, A. J. Heeger, *Phys. Rev. B* **1998**, 58, 7035;

[43] J. D. Joannopoulos, R. D. Meade, J. N. Winn, *Photonic Crystals: molding the flow of light*, Princeton University Press, Princeton, NJ, **1995**;

[44] P. N. Prasad, *Nanophotonics*, John Wiley & Sons, Hoboken, NJ, **2004**;

[45] Lopez C., *Adv. Mater.* **2003**, 15, 1679;

[46] J. E. G. J. Wijnhoven, W. L. Vos, *Science* **1998**, 281, 802;

[47] K. Sakoda, *Optical Properties of Photonic Crystals*, Springer, Berlin, **2001**;

[48] L. Guidoni, C. Triche, P. Verkerk, G. Grynberg, *Phys. Rev. Lett.* **1997**, 79, 3363;

[49] R. C. Gauthier, A. Ivanov, *Opt. Express* **2004**, 12, 990;

[50] C. E. Lee, C. F. Lai, Y. C. Lee, H. C. Kuo, T. C. Lu, S. C. Wang, *IEEE Photonic. Tech. L.* **2009**, 21, 331;

[51] M. Notomi, H. Suzuki, T. Tamamura, K. Edagawa, *Phys. Rev. Lett.* **2004**, 92, 123906;

[52] V. S. Letokhov, *Zh. Eksp. Teor. Fiz.* **1967**, 53, 1442;

[53] V. S. Letokhov, *Sov. Phys. JETP* **1968**, 26, 835;

[54] C. Gouedard, D. Husson, C. Sauteret, F. Auzel, A. Migus, *J. Opt. Soc. Am. B* **1993**, 10, 2358;

[55] N. M. Lawandy, R. M. Balachandran, A. S. L. Gomes, E. Sauvain, *Nature* **1994**, 368, 436;

[56] H. Cao, Y. G. Zhao, S. T. Ho, E. W. Seelig, Q. H. Wang, R. P. H. Chang, *Phys. Rev. Lett.* **1999**, 82, 2278;

[57] H. Cao, Y. G. Zhao, S. T. Ho, E. W. Seelig, X. Liu, R. P. H. Chang, *Phys. Rev. Lett.* **2000**, 84, 5584;

[58] S. Gottardo, S. Cavalieri, O. Yaroschuck, D. S. Wiersma, *Phys. Rev. Lett.* **2004**, 93, 263901;

[59] D. S. Wiersma, S. Cavalieri, *Nature* **2001**, 414, 708;

[60] A. Andreev, F. Quochi, F. Cordella, A. Mura, G. Bongiovanni, H. Sitter, G. Hlawacek, C. Teichert, N. S. Sariciftci, *J. Appl. Phys.* **2006**, 99, 034305;

[61] F. Quochi, F. Cordella, A. Mura, G. Bongiovanni, F. Balzer, H.-G. Rubahn, *Appl. Phys. Lett.* **2006**, 88, 041106;

[62] F. Quochi, F. Cordella, A. Mura, G. Bongiovanni, F. Balzer, H.-G. Rubahn, *J. Phys. Chem. B* **2005**, 109, 21690;

[63] F. Quochi, A. Andreev, F. Cordella, R. Orrù, A. Mura, G. Bongiovanni, H. Hoppe, H. Sitter, N. S. Sariciftci, *J. Of Lumin.* **2005**, 112, 321;

[64] F. Quochi, F. Cordella, R. Orrù, J.E. Communal, P. Verzeroli, A. Mura, G. Bongiovanni, A. Andreev, H. Sitter, N.S. Sariciftci, *Appl. Phys. Lett.* **2004**, 84, 4454;

[65] V. Milner, A. Z. Genack, *Phys. Rev. Lett.* **2005**, 94, 073901;

[66] R. C. Polson, Z. V. Vardeny, *Appl. Phys. Lett.* **2004**, 85, 1289;

[67] R. Choe, A. Corlu, K. Lee, T. Durduran, S. D. Konecky, M. Grosicka-Koptyra, S. R. Arridge, B. J. Czerniecki, D. L. Fraker, A DeMichele, B. Chance, M. A. Rosen, A. G. Yodh, *Med. Phys.* **2005**, 32, 1128;

[68] G. R. Williams, S. B. Bayram, S. C. Rand, T. Hinklin, R. M. Laine, *Phys. Rev. A* **2001**, 85, 013807;

[69] S. Gottardo, R. Sapienza, P. D. Garcia, A. Blanco, D. S. Wiersma, C. Lopez, *Nat. Photonics* **2008**, 2, 429;

[70] P. D. Garcia, M. Ibisite, R. Sapienza, D. S. Wiersma, C. Lopez, *Phys. Rev. A* **2009**, 80, 013833;

[71] M. D. McGehee, M. A. Diaz-Garcia, F. Hide, R. Gupta, E. K. Miller, D. Moses, A. J. Heeger, *Appl. Phys. Lett.* **1998**, 72, 1536;

[72] G. A. Turnbull, T. F. Kauss, W. L. Barnes, I. D. W. Samuel, *Synth. Met.* **2001**, 121, 1757;

[73] G. A. Turnbull, P. Andrew, M. J. Jory, W. L. Barnes, I. D. W. Samuel, *Phys. Rev. B* **2001**, 6412, 125122;

[74] W. Holzer, A. Penzkofer, T. Pertsch, N. Danz, A. Brauer, E. B. Kley, H. Tillmann, C. Bader, H. H. Horhold, *Appl. Phys. B: Lasers Opt.* **2002**, 74, 333;

[75] P. Andrew, G. A. Turnbull, I. D. W. Samuel, W. L. Barnes, *Appl. Phys. Lett.* **2002**, 81, 954;

[76] T. Matsui, M. Ozaki, K. Yoshino, F. Kajzar, *Jpn. J. Appl. Phys. Part 2* **2002**, 41, L1386;

[77] T. Riedl, T. Rabe, H. H. Johannes, W. Kowalsky, J. Wang, T. Weimann, P. Hinze, B. Nehls, T. Farrell, U. Scherf, *Appl. Phys. Lett.* **2006**, 88, 241116;

[78] G. Heliotis, R. D. Xia, G. A. Turnbull, P. Andrew, W. L. Barnes, I. D. W. Samuel, D. D. C. Bradley, *Adv. Funct. Mater.* **2004**, 14, 91;

[79] C. Karnutsch, C. Gyrtner, V. Haug, U. Lemmer, T. Farrell, B. S. Nehls, U. Scherf, J. Wang, T. Weimann, G. Heliotis, C. Pflumm, J. C. deMello, D. D. C. Bradley, *Appl. Phys. Lett.* **2006**, 89, 201108;

[80] C. Kallinger, M. Hilmer, A. Haugeneder, M. Perner, W. Spirkl, U. Lemmer, J. Feldmann, U. Scherf, K. Mullen, A. Gombert, V. Wittwer, *Adv. Mater.* **1998**, 10, 920;

[81] M. Berggren, A. Dodabalapur, R. E. Slusher, A. Timko, O. Nalamasu, *Appl. Phys. Lett.* **1998**, 72, 410;

[82] A. Dodabalapur, M. Berggren, R. E. Slusher, Z. Bao, A. Timko, P. Schiortino, E. Laskowski, H. E. Katz, O. Nalamasu, *IEEE J. Sel. Top. Quantum Electron.* **1998**, 4, 67;

[83] D. Pisignano, M. Anni, G. Gigli, R. Cingolani, G. Barbarella, L. Favaretto, G. B. V. Sotgiu, *Synth. Met.* **2003**, 137, 1057;

[84] D. Pisignano, L. Persano, P. Visconti, R. Cingolani, G. Gigli, G. Barbarella, L. Favaretto, L. *Appl. Phys. Lett.* **2003**, 83, 2545.

[85] D. Pisignano, L. Persano, E. Mele, P. Visconti, M. Anni, G. Gigli, R. Cingolani, L. Favaretto, G. Barbarella, *Synth. Met.* **2005**, 153, 237;

[86] D. Pisignano, L. Persano, E. Mele, P. Visconti, R. Cingolani, G. Gigli, G. Barbarella, L. Favaretto, *Opt. Lett.* **2005**, 30, 260;

[87] S. G. Johnson, J. D. Joannopoulos, Optics Express, 8, 173 (2001);

[88] C. S. Lien, *Physics of Optoelectronic Devices*, John Wiley & Sons, New York, **1995**;

[89] J. M. Weissman, H. B. Sunkara, A. S. Tse, S. A. Asher, *Nature* **1996**, 274, 959;

[90] J. H. Holtz, S. A. Asher, *Nature* **1997**, 389, 829;

[91] V. S. Y. Lin *et al*, *Science* **1997**, 278, 840;

[92] Y. Y. Li *et al*, *Science* **2003**, 299, 2045;

[93] Z.-Z. Gu, T. Iyoda, O. Sato, *J. Am. Chem. Soc.* **2000**, 122, 12387;

[94] S. H. Foulger *et al.*, *Adv. Mater.* **2001**, 13, 1898;

[95] J. D. Debord, L. A. Lyon, *J. Phys. Chem. B* **2000**, 104, 6327;

[96] M. Ozaki, Y. Shimoda, M. Kasano, K. Yoshino, *Adv. Mater.* **2002**, 14, 514;

[97] Z.-Z. Gu, T. Iyoda, A. Fujishima, O. Sato, *Adv. Mater.* **2001**, 13, 1295;

[98] Z. Hu, X. Lu, J. Gao, *Adv. Mater.* **2001**, 13, 1708;

[99] H. Fudouzi, Y. Xia, *Adv. Mater.* **2003**, 15, 892;

[100] K. Busch, S. John, *Phys. Rev. Lett.* **1999**, 83, 892;

[101] Y. Kang, J. J. Walish, T. Gorishnyy, E. L. Thomas, *Nat. Mater.* **2007**, 6, 957;

[102] J. Yoon, W. Lee, E. L. Thomas, *Macromol.* **2008**, 41, 4582;

[103] A. Rose, Z. Zhu, C. F. Madigan, T. M. Swager, V. Bulovic, *Nature* **2005**, 434, 876;

[104] H. Du, R. A. Fuh, J. Li, A. Corkan, J. S. Lindsey, *Photochemistry and Photobiology* **1998**, 68, 141;

[105] M. Montalti, A. Credi, L. Prodi, M. T. Gandolfi, in *Handbook of photochemistry* (3rd ed.), Taylor & Francis, Boca Raton FL, **2006**, p. 325;

[106] U. H. F. Bunz in Conjugated *Polymers: Theory, Synthesis, Properties, and Characterization*, CRC Press Florida, USA, **2007**;

[107] http://www.texloc.com/closet/cl_refractiveindex.html;

[108] B. O'Regan, M. Gratzel, *Nature (London)* **1991**, *75*, 1896;

[109] http://en.wikipedia.org/wiki/Spin_coating;

[110] www.quantasystem.com, *Near Diffraction Limited Q-Switched Nd:YAG Laser (Laser User Manual)*, **1999**;

[111] F. Scotognella, A. Monguzzi, M. Cucini, F. Meinardi, D. Comoretto, R. Tubino, Int. J. Photoenergy, **2008**;

[112] K. Kuriki, T. Kobayashi, N. Imai, T. Tamura, S. Nishihara, Y. Nishizawa, A. Tagaya, Y. Koike, *Appl. Phys. Lett.* **2000**, 77, 331;

[113] F. Scotognella, A. Monguzzi, F. Meinardi, R. Tubino, *Phys. Chem. Chem. Phys.*, *accepted*;

[114] M. Ghulinyan, C.J. Oton, L. Dal Negro, L. Pavesi, R. Sapienza, M. Colocci, D. S. Wiersma, Phys. Rev. B, **2005**, 71, 094204;

[115] G. A. Ozin, K. Hou, B. V. Lotsch, L. Cademartiri, D. P. Puzzo, F. Scotognella, A. Ghadimi, J. Thomson, *Materials Today* **2009**, 12, 12;

[116] D. R. Gagnon, J. D. Capistran, F. E. Karasz, R. W. Lenz, S. Antoun, *Polymer* **1987**, 28, 567;

[117] X-ray data were collected on a Bruker-Nonius Kappa-CCD diffractometer using monochromated Mo-Kα radiation and were measured using a combination of ϕ scans and ω scans with κ offsets, to fill the Ewald sphere. The data were processed using the Denzo-SMN package [118]. Absorption corrections were carried out using SORTAV [119]. The structure was solved and refined using SHELXTL V6.1 [120] for full-matrix least-squares refinement that was based on F^2. All H atoms bonded to C atoms were included in calculated positions and allowed to refine in riding-motion approximation with U~iso~tied to the carrier atom. H atoms bonded to the O atoms were refined independently with isotropic displacement parameters;

[118] Otwinowski, Z. & Minor, W. (1997). Methods in Enzymology, Vol. 276, Macromolecular Crystallography, Part A edited by C. W. Carter & R. M. Sweet pp. 307-326. London: Academic press;

[119] Blessing, R. H. (1995). Acta Cryst. A51, 33-38;

[120] Sheldrick, G. M. (2008). Acta Cryst. A64, 112-122;

[121] D. P. Puzzo, F. Scotognella, M. Zavelani-Rossi, M. Sebastian, A. J. Lough, I. Manners, G. Lanzani, R. Tubino, G. A. Ozin, *Nano Lett.* **2009**, 10.1021/nl902516t;

[122] H. Takeuchi, K. Natsume, S. Suzuki, H. Sakata, *Electron. Lett.* **2007**, 43, 1.